In search of a unifying theory of white matter aging: tract morphometry-microstructure relationships

Tyler D. Robinson[1], Yutong L. Sun[1], Paul T. H. Chang[1], J. Jean Chen[1,2,3]

1. Rotman Research Institute, Baycrest, Canada
2. Medical Biophysics, University of Toronto, Canada
3. Biomedical Engineering, University of Toronto, Canada

ABSTRACT

Progressive age-related changes in white matter morphometry and microstructure have been found throughout the brain. Both declines in white matter (WM) volume and deterioration of microstructural integrity have been observed. Predicting these changes across WM tracts and building an integrated model of age-related WM trajectories has proven challenging. While tractwise differences in volume and microstructural declines are common targets of investigation, there has been relatively little exploration into other attributes of tract morphology or its relation to microstructural measures in vivo. This study seeks to examine ten WM tracts for tract-wise differences in WM volume, length, the ratio of volume to length (VLR), and microstructural integrity as measured by fractional anisotropy (FA), mean diffusivity (MD), axial diffusivity (AD), and radial diffusivity (RD) using diffusion MRI data from the Human Connectome Project in Aging (HCP-A). From these measures, we analyzed relationships between morphometry and microstructure in the aging brain with the goal of laying the foundation for a unified model of age-related changes that relates WM microstructure/morphometry and developmental trajectories. Results indicated wide variation in rates and patterns of decline between tracts, as well as tract-specific interactions between tract morphometry and microstructure. Robust sex differences were also identified. Our findings demonstrate the need for further exploration of the mechanisms behind both macro- and microstructural differences across the aging brain.

INTRODUCTION

Changes in function, structure, and microstructure in the human brain occur throughout the adult lifespan (Baker et al., 2014; Bartzokis, 2004; Bookheimer et al., 2019; Buyanova & Arsalidou, 2021; Chad et al., 2018; Kiely et al., 2022; Kodiweera et al., 2016; Piguet et al., 2009). Evidence suggests that early microstructural degeneration can be observed in the white matter (WM) prior to their emergence in cortical regions (Debette & Markus, 2010; Hu et al., 2021; Madden et al., 2012; Seiler et al., 2018). Earlier prediction of regional declines is invaluable to medical intervention for the postponement or reversal of progressive cognitive and structural decline (de Groot et al., 2015). Consistent changes in white matter macro-/microstructure and histology have been demonstrated in advancing age (Baker et al., 2014; Bastin et al., 2010; Choy et al., 2020; Ouyang et al., 2021; Tang et al., 1997), with overall volume decreases identified in normal aging (Bastin et al., 2010; Piguet et al., 2009; Tang et al., 1997). Notably, WM volume decreases by up to 28% in adult aging (Pakkenberg & Gundersen, 1997), but there is still a limited understanding of the microstructural variations underlying this volume reduction. In order to understand the mechanisms underlying WM decline, it is important to incorporate knowledge of age-related changes in WM morphometry and microstructure (Bartzokis, 2004; Benitez et al., 2018; Maffei et al., 2021; Yendiki et al., 2011). In turn, examining the relationship between this interaction and the WM developmental trajectory can help further elucidate the processes that govern WM degeneration in aging. Building a more comprehensive modeling of age-related WM changes offers a tool to detect degeneration at earlier stages.

While WM volume loss in aging has been established, the regional distribution of this volume loss is as of yet under-defined. Decreases in cumulative fiber length (i.e. the total length across the brain as extrapolated from histological samples) have been observed in both humans and animals using diffusion MRI and microscopy, respectively (Baker et al., 2017; Marner et al., 2003). This loss can in part be attributed to the preferential culling of vulnerable axons, as fibers with lower axon diameter and less dense myelin sheaths are notably more vulnerable to this process (Tang et al., 1997). This further suggests that a significant contributor to WM morphometrical losses in aging may be a reduction in the total number of fibers and a concomitant increase in mean axon diameter in surviving tissue, as opposed to changes in the length of surviving axons. As WM fibers with higher diameter are also typically higher in length (Liewald et al., 2014), aging tracts should demonstrate increases in length relative to volume as shorter, narrower fibers are culled and the longer surviving fibers comprise a greater portion of the WM tissue. However, to what degree this potential effect contributes to changes in WM volume, considering the general atrophy of brain volume with age (Azevedo et al., 2019; Fjell et al., 2009, 2014; Sala et al.,

2012), is unclear. Individual fiber tracts in the white matter exhibit varying degrees of vulnerability to age-related fiber culling (Choy et al., 2020), potentially giving rise to previous observations of both decreasing and increasing fiber length in specific major white matter bundles including the splenium and superior longitudinal fasciculus (Ouyang et al., 2021), calling into question the assumption that overall decreases in fiber length correspond to regional decreases in tract length. Moreover, the tools with which living WM can be accurately delineated into discrete tracts are both relatively new and continually improving (Maffei et al., 2021). Alternate mechanisms of shortening in measurable fibre length, such as damage and delayed clearing of remaining debris (Avellino et al., 1995) or the presence of early-stage degenerative conditions targeting short-range structural connections (Wu et al., 2022) may also influence measures of mean tract length. Morphometrical research has noted cross-sectional tract-wise differences in age-related decline with regards to volume and microstructure (Bastin et al., 2010; Choy et al., 2020), but in the context of aging, it is also important to assess normalized fibre length in order to account for sex differences and age-related general atrophy, thereby gleaning the proportional instead of absolute changes in different WM tracts (Bajada et al., 2019). As many existing works do not address potential sex differences, distinctions between sex-specific trajectories of decline remain unclear.

To expand beyond morphometric observations, diffusion MRI metrics such as fractional anisotropy (FA) and mean diffusivity (MD) offer proxy measures for WM microstructural integrity (Madden et al., 2012; Stadlbauer et al., 2008). Phenomena such as culling of axonal fibers and demyelination of surviving axons results in measurable changes in diffusion, such that mean diffusivity increases and fractional anisotropy decreases as axon bundles become less dense (Choy et al., 2020; Fan et al., 2019; Kodiweera et al., 2016). Declines in microstructural integrity in aging WM are associated with both WM hyperintensities and implicated in declining cognitive performance (Debette & Markus, 2010; Hu et al., 2021). Existing research has also identified heterogeneous rates of decline in different WM regions, such as sections of the corpus callosum, and broader anterior and posterior regions of the brain (C. L. Armstrong et al., 2004; Brickman et al., 2012; Fan et al., 2019; Kiely et al., 2022; Seiler et al., 2018). This knowledge is of considerable interest for anticipating pathological changes and prioritizing interventions (Debette & Markus, 2010). Tract-wise studies and inter-tract comparisons of WM microstructural variations in aging remain limited.

We reasonably expect microstructural variations to underlie morphometrical variations in aging (N. M. Armstrong et al., 2020; Hoagey et al., 2019; Taki et al., 2011), but interaction between morphometrical and microstructural declines represents another sparsely addressed topic (Bastin et al., 2010; Kezele et al., 2008; Seiler et al., 2018). Prior investigation notes a decrease in overall fiber count with age that could account for measurable changes in WM volume (Marner et al., 2003). This would pose microstructural declines as a direct cause of morphometrical changes in volume. However,

histological findings also note that surviving WM fibers are thicker with advancing age (Fan et al., 2019, 2020). Moreover, while age may result in lower density in fiber bundles (Choy et al., 2020; Fan et al., 2019; Kiely et al., 2022; Marner et al., 2003), changes in density may not necessitate uniform decreases in volume, as space within fiber bundles is occupied by intercellular fluid (Kodiweera et al., 2016). Uncertainty in these processes make it difficult to anticipate the relationships between microstructural decline and changing WM morphometry with age. This study sought to map changes in WM morphometry and microstructure, examine their interactions, and compare those changes across individual WM tracts. Tractwise FA and MD, as well as axial diffusivity (AD) and radial diffusivity (RD) are used as the target microstructural metrics of this study. The morphometry of each tract is quantified in measures of tractwise mean length, volume, and volume-length ratio, and these are, in turn, compared to the microstructural measures. We hypothesize that: (1) age-related microstructural differences will be greater in tracts that demonstrate greater age-related morphometrical differences, and (2) given patterns of preferential WM fiber culling (Marner et al., 2003; Tang et al., 1997), and associations between axon diameter and axon length (Liewald et al., 2014), tracts that become relatively thinner with age will also have relatively high mean tract lengths.

METHODS

Subjects and data acquisition

This study involved data from five hundred and thirty-five healthy adult subjects (300 female, aged 36-100 years) of the Human Connectome Project in Aging (HCP-A) dataset (OMB Control# 0925-0667) (Bookheimer et al., 2019; Harms et al., 2018). Of this sample, thirty-two subjects were excluded due to MRI artifacts resulting in notable errors when producing WM masks. An additional three subjects (100 years of age) were excluded as outliers. This resulted in a final sample size of 500 subjects (294 female, aged 36-89). All subjects were in good health and without pathological cognitive impairment (i.e. stroke, clinical dementia).

Each data set included a whole-WM T1-weighted structural MRI (0.8 mm isotropic resolution) and diffusion-weighted MRI (dMRI), collected on one of four matched Siemens Prisma 3T MRI scanners, with a 1.5 mm isotropic voxel resolution, MB=4, with 93 directions at b=1500s/mm^2. Further parameters for structural and diffusion image acquisition can be found in (Harms et al., 2018).

Image analysis

dMRI data were corrected for eddy-current and susceptibility-related distortions via EDDY. Diffusion data were used to identify and reconstruct eighteen major white matter tracts using the Tracts Constrained by Underlying Anatomy (TRACULA) tool in Freesurfer version 7.2.0. FMRIB Software Library version

6.0.5 (FSL)'s fslmaths function was then used to produce per subject masks of each WM tract in local space. A 99th percentile voxelwise apparent diffusion coefficient (ADC) intensity threshold was applied to the generated tracts to exclude potential outliers, followed by a 20% threshold on the resulting masks to generate the final masked regions of interest (ROI) used throughout this study. The eighteen reconstructed tracts were collapsed bilaterally to produce ten tracts of interest: The forceps major (Fmajor), forceps minor (Fminor), anterior thalamic radiation (ATR), Cingulum Angular Bundle (CAB), Cingulate Gyrus (CCG), Corticospinal Tract (CST), Inferior Longitudinal Fasciculus (ILF), Superior Longitudinal Fasciculus Parietal (SLFP), Superior Longitudinal Fasciculus Temporal (SLFT), and the Uncinate Fasciculus (UNC). In single tract analyses, Rosner's tests were performed to identify and exclude volume outliers per tract. The resulting subject counts were as follows: Fmajor (N=493), Fminor (N=493), ATR (N=497), CAB (N=490), CCG (N=495), CST (N=491), ILF (N=497), SLFP (N=497), SLFT (N=495), and UNC (N=495).

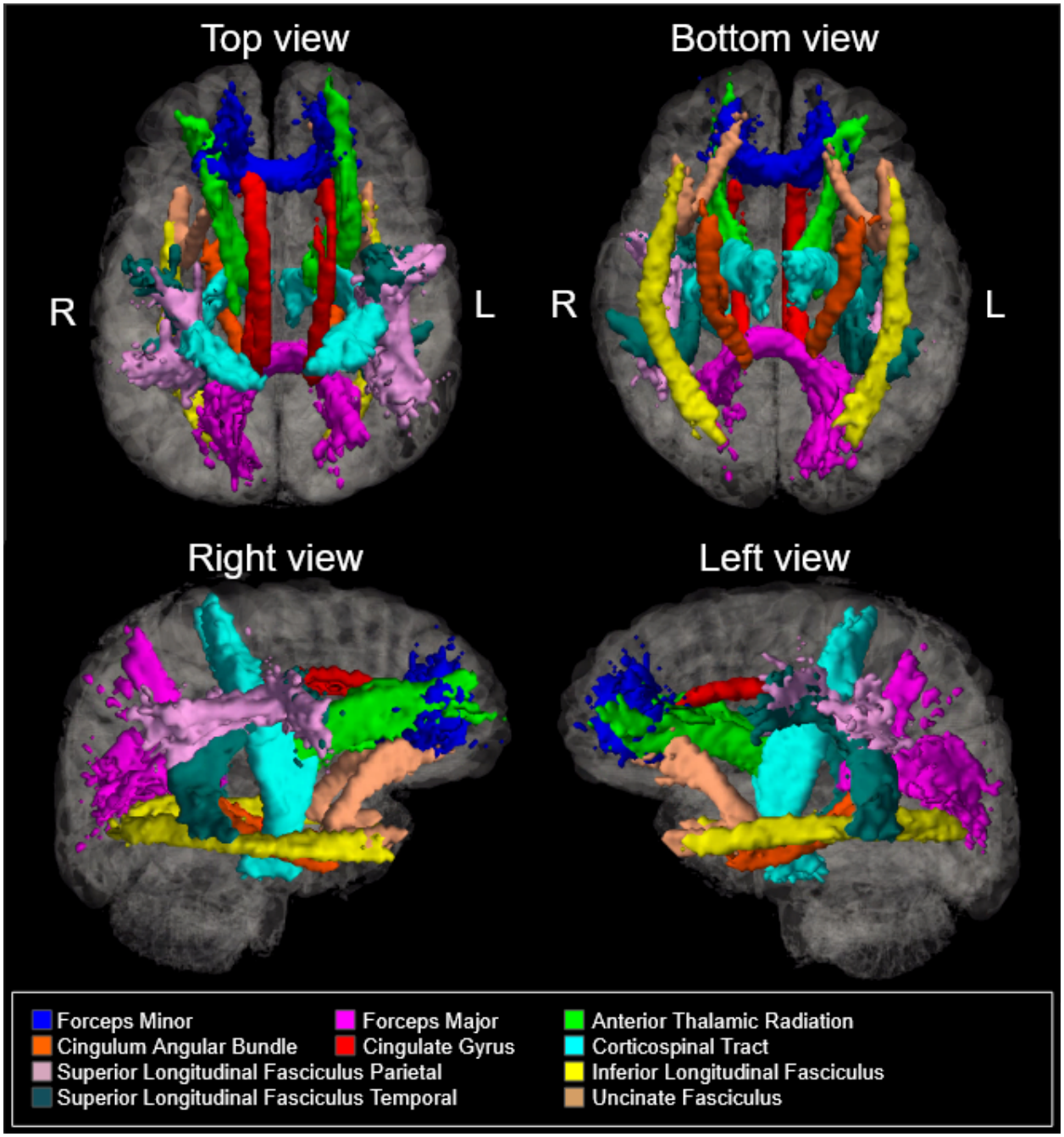

Figure 1: Ten bilateral tracts of interest reconstructed Freesurfer's TRACULA package

Morphometry

From these masked regions, morphometry measures were calculated for tract volume, length, and volume-to-length ratio (VLR):

1. Tract volume:

   a. Raw tract volume ("Volume"): calculated as the total number of voxels ($2x2x2mm^3$) included in each masked tract region.
   b. Normalized tract volume ("$Volume_{norm}$"): calculated as tract volume divided by subject-specific intracranial volumes (ICV). This represents the tract volume as a percentage of the brain volume, thereby reducing the effect of inherent inter-subject variability in tissue volumes.
   c. Percent tract volume change ("$Volume_{perc}$"): calculated as individual raw tract volume divided by the mean raw tract volume of the youngest 10% of subjects.
2. Tract length
   a. Raw tract length ("Length"): calculated as the mean streamline length from 1500 streamlines per tract in TRACULA.
   b. Normalized tract length ("$Length_{norm}$"): the raw tract length divided by the length of an subject-specific length of age-stable white matter tract (the cingulate gyrus (CCG)), as identified from its relatively stable raw tract length identified in the raw values. This reduces the effect of inherent inter-subject variability in tract lengths.
   c. Percent tract length change ("$Length_{perc}$"): calculated as individual raw tract length divided by the mean raw tract length of the youngest 10% of subjects.
3. Tract volume-to-length ratio (VLR)
   a. Raw VLR ("VLR"): calculated as the ratio of tract volume to length. This represents the "thinness" of a tract relative to a reference tissue.
   b. Normalized VLR ("VLR_{norm}"): calculated as the ratio of ICV-corrected tract volume to CCG-corrected tract length. This represents the "thinness" of a tract relative to a reference tissue.
   c. Percent tract VLR change ("VLR_{perc}"): calculated as individual raw tract VLR divided by the mean raw tract VLR of the youngest 10% of subjects.

Microstructure

Fractional Anisotropy (FA), Mean Diffusivity MD, Axial Diffusivity (AD), and Radial Diffusivity (RD) maps were derived using Dipy's DKI tool, to provide kurtosis-corrected DTI metrics (given the high b-value used in the HCP-A dMRI acquisitions). Tract masks generated in the morphometric assessment were applied to the local space diffusion images using fslmaths to generate mean FA and mean diffusivity values for each tract of interest of each participant. As with morphometric measures, baseline normalized values ("FA_{perc}", "MD_{perc}", "AD_{perc}", "RD_{perc}") were calculated for each microstructural measure to determine percent difference from the youngest 10% of the sample.

Statistical analyses

Morphometry

In these analyses we assessed the relationships between morphometry, age and sex using multivariate linear and quadratic regression. All analyses in this study were conducted in R (version 4.1.1). First, between-subjects ANOVA was used to determine the presence of sex differences in tract specific $Length_{norm}$, $Volume_{norm}$, and VLR_{norm}. Age was then regressed onto whole-WM mean $Length_{norm}$, whole-WM total $Volume_{norm}$, and whole-WM mean VLR_{norm} with sex as a variable of no interest. Subsequent assessment of sex differences in mean morphometry was conducted via sequential multivariate regressions of sex onto mean tract length, total tract volume, and mean tract VLR using age as a covariate of no interest.

Following whole-WM analyses, age was separately regressed onto tractwise $Length_{perc}$, $Volume_{perc}$, and VLR_{perc} values for each of the ten reconstructed tracts. As in the whole-WM analyses, sex was used as a covariate of no interest. Subsequent multivariate regressions of sex onto normalized morphometric values were performed, using age as a covariate of no interest. False detection rate (FDR) adjustment was applied to all resulting p-values to correct for multiple comparisons.

Microstructure

Whole-WM age-related microstructure differences were assessed via multivariate regression by first regressing age onto mean MD_{perc} and mean FA_{perc} values derived from voxel-count weighted tract MD_{perc} and FA_{perc} averages using sex as a covariate of no interest. Subsequent assessment of sex differences in microstructure was conducted via sequential multivariate regressions of sex on to mean MD_{perc} and mean FA_{perc}, using age as a covariate of no interest.

Sequential multivariate regressions were also used to assess tractwise age-related differences in microstructure, with age regressed onto MD_{perc}/FA_{perc} for each of the ten tracts using sex as a covariate of no interest. Sex was subsequently regressed onto MD_{perc}/FA_{perc} for each of the ten tracts using age as a regressor of no interest. FDR adjustment was again applied to the resulting p-values.

Morphometry vs. microstructure

Two multivariate regression models were constructed to assess the relationships between morphometry, microstructure, age, and sex in our sample. These models were first applied to whole-WM $Length_{perc}$ and VLR_{perc} values, then to the individual values for each tract of interest:

- *Model 1. microstructure vs. morphometry across ages:* assesses the degree to which morphometric metrics account for the age-related variability in mean normalized tract length, volume, and VLR, with subject sex as a covariate of no interest. That is,
    - $\{FA_{perc}, MD_{perc}\} = f(Length_{perc}+Sex)$
    - $\{FA_{perc}, MD_{perc}\} = f(VLR_{perc}+Sex)$

- *Model 2. microstructure vs. morphometry between sexes:* assess the degree to which morphometric metrics account for sex-related differences in normalized tract length, volume and VLR, with subject age as a covariate of no interest. That is,
    - $\{FA_{perc}, MD_{perc}\} = f(Length_{perc}+Age)$
    - $\{FA_{perc}, MD_{perc}\} = f(VLR_{perc}+Age)$
    - One set of models is produced for each sex.

Canonical Correlation Analysis

Canonical correlation analysis (CCA) was conducted to examine the degrees to which our variables of interest contributed to age-related differences in morphometry and microstructure respectively. Two column vectors were computed using our morphometric (V_1) variables ($Length_{perc}$, $Volume_{perc}$) and microstructural (U_1) variables (AD_{perc}, RD_{perc}, FA_{perc}) in Matlab. The linear combinations of V and U vectors which produced the highest correlation were then calculated to determine on a tractwise basis which variables loaded most strongly to age differences by tract. This and following analyses substituted AD and RD variables for the MD variable used in previous analyses as examining the axes of diffusion separately was necessary to clarify relationships between FA and other diffusion metrics as they relate to microstructural deterioration.

Cross-Correlation Analysis

Cross-correlations functions (CCF) were calculated in Matlab to determine the presence of age-lagged relationships between morphometry and microstructure, as well as between measures within each category. To reduce ambiguity in the CCF interpretation, only variables demonstrating significant non-linear age effects on a tractwise basis were examined in this analysis, using a curvature threshold of 0.0005. CCFs were calculated based on the models of age effects on six paired tractwise microstructure/morphometry measures, along with cross-comparisons for AD_{perc}/RD_{perc} vs FA_{perc} and $Length_{perc}$ vs $Volume_{perc}$:

- Length/Microstructure
    - $Length_{perc}$ vs AD_{perc}
    - $Length_{perc}$ vs RD_{perc}
    - $Length_{perc}$ vs FA_{perc}
- Volume/Microstructure
    - $Volume_{perc}$ vs AD_{perc}
    - $Volume_{perc}$ vs RD_{perc}
    - $Volume_{perc}$ vs FA_{perc}

- AD_{perc} vs FA_{perc}
- RD_{perc} vs FA_{perc}
- $Length_{perc}$ vs $Volume_{perc}$

RESULTS

Morphometry

Age Differences:

Negative associations were observed between age and both whole-WM mean $Length_{norm}$ ($F(2, 497) = 66.8$, $p < .001$, $R^2_{Adjusted} = .21$, slope = -0.1mm/year) and whole-WM $Volume_{norm}$ ($F(2, 497) = 84.9$, $p < .001$, $R^2_{Adjusted} = .25$, slope = -288.4 mm^3/year) when controlling for sex. Similarly, age and mean tract VLR_{norm} are significantly and negatively associated ($F(2, 497) = 72.4$, $p < .001$, $R^2_{Adjusted} = .22$, slope = -0.27 mm^2/year) when controlling for sex.

Negative relationships between age and tract $Length_{norm}$ were identified in Fminor, CAB, CST, ILF, SLFP, SLFT, and UNC. Negative relationships between age and tract $Volume_{norm}$ were identified in Fmajor, Fminor, ATR, CAB, CCG, ILF, SLFP, SLFT, and UNC. Negative tractwise relationships between age and tract VLR_{norm} were observed in the Fmajor, the Fminor, ATR, CAB, CCG, and UNC (Figure 4).

Sex Differences:

Male subjects demonstrated greater mean tract $Length_{norm}$ ($F(2, 497) = 66.8$, $p < .001$, $R^2_{Adjusted} = .21$, effect = 3.0mm), $Volume_{norm}$ ($F(2, 497) = 84.9$, $p < .001$, $R^2_{Adjusted} = .25$, effect =16428.3 mm^3), and VLR_{norm} values ($F(2, 497) = 72.4$, $p < .001$, $R^2_{Adjusted} = .22$, effect = 21.5 mm^3/mm) across tracts when controlling for the effects of age.

Female subjects demonstrated higher tract $Length_{norm}$ in the CST, while male subjects demonstrated higher $Length_{norm}$ in the Fmajor, Fminor, ATR, CCG, ILF, SLFP, SLFT, and UNC. Male subjects also showed significantly higher $Volume_{norm}$ and VLR_{norm} in all ten tracts of interest (Figure 2).

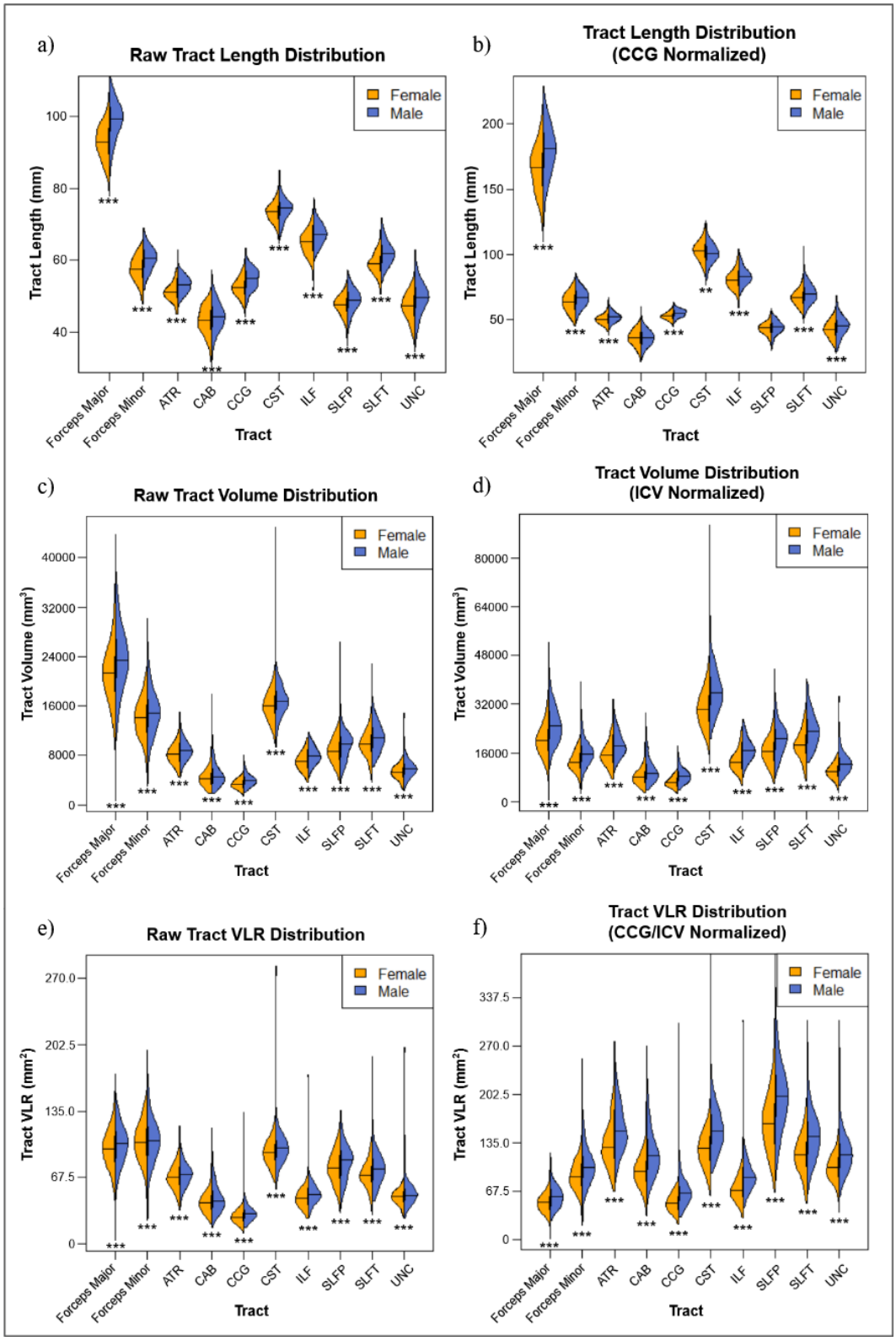

Figure 2: Tractwise raw Length, Volume, and VLR (a, c ,e) and Length$_{norm}$, Volume$_{norm}$, and VLR$_{norm}$ (b, d, f) distributions separated by sex.

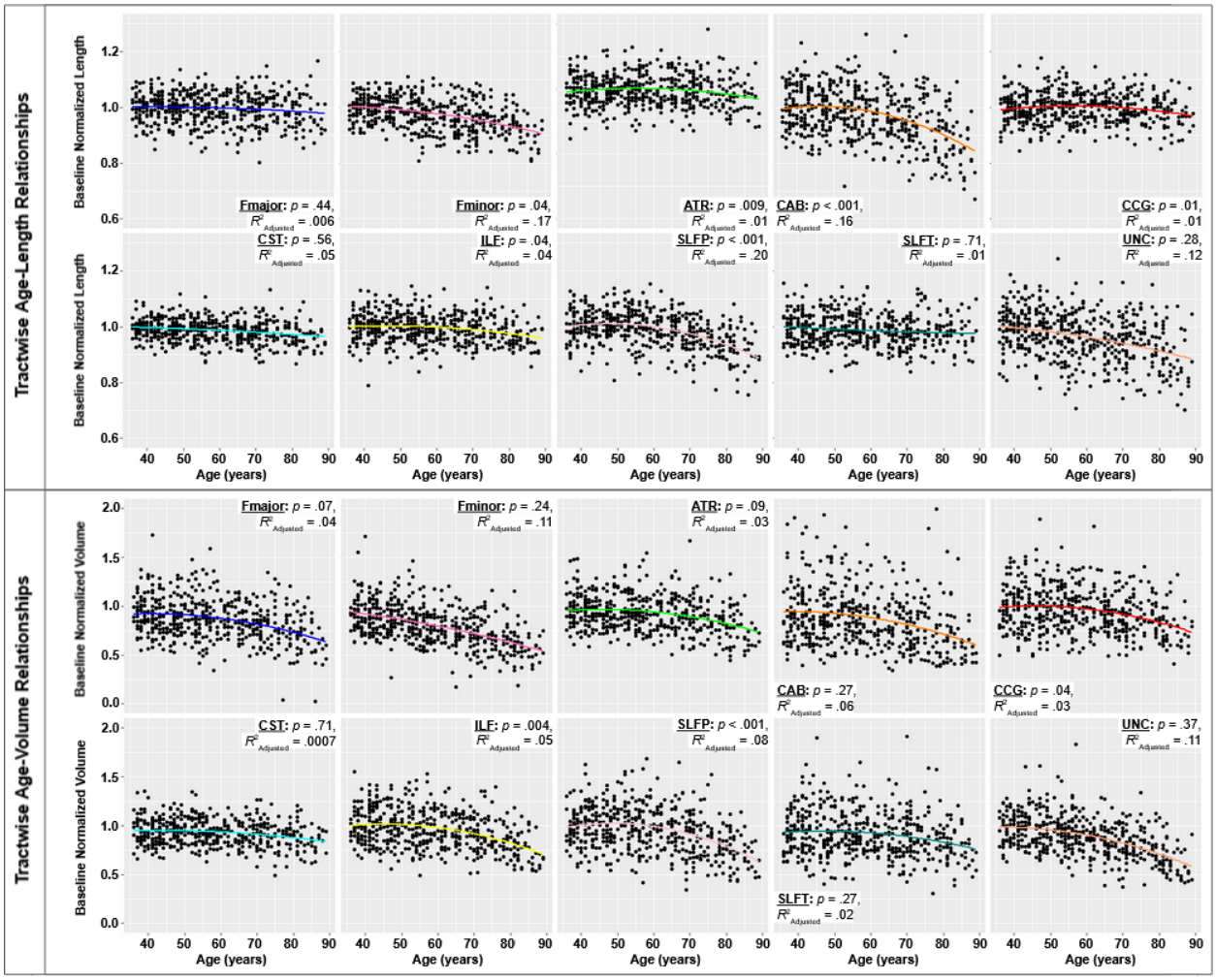

Figure 3: Tractwise quadratic regression of age effects on $Length_{perc}$ and $Volume_{perc}$

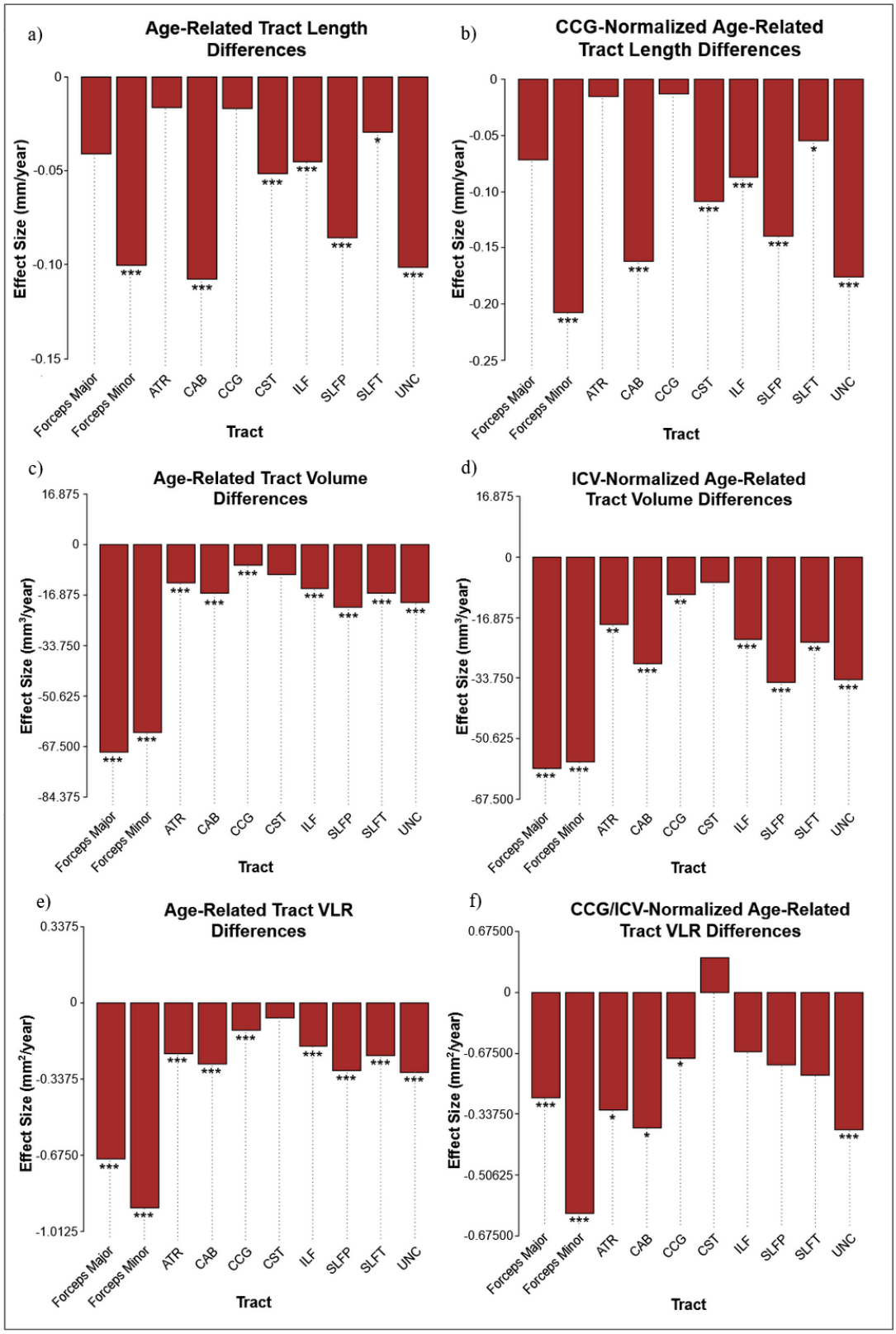

Figure 4: Tractwise age effects on raw Length, Volume, and VLR (a, c ,e) and $Length_{norm}$, $Volume_{norm}$, *and* VLR_{norm} *(b, d, f).*

Microstructure

MD/FA vs. Age/Sex:

Age demonstrated a significant positive association with mean MD_{perc} ($F(2, 497) = 78.58$, $p < .001$, $R^2_{Adjusted} = .24$, effect = 0.0013 mm^2/s). Age also demonstrated a significant negative association with mean FA_{perc} ($F(2, 497) = 9.77$, $p < .001$, $R^2_{Adjusted} = .03$, effect = -0.00077), such that the value of mean WM FA_{perc} decreased by 0.08% per year of age. Female subjects exhibited higher mean MD_{perc} ($F(2, 497) = 78.58$, $p < .001$, $R^2_{Adjusted} = .24$, effect: 0.0078).

All ten tracts of interest showed significant positive relationships between age and MD_{perc} (Figure 5). Age was significantly negatively related to FA_{perc} in the Fmajor, Fminor, ATR, CAB, CCG, ILF, and SLFP. Female subjects demonstrated significantly higher MD_{perc} in the CST ($F(2, 497) = 47.0$, $p < .001$, $R^2_{Adjusted} = .16$, effect = 0.000028 mm^2/s) and in the UNC ($F(2, 497) = 71.2$, $p < .001$, $R^2_{Adjusted} = .22$, effect = 0.0000076 mm^2/s) In the ILF, men demonstrated significantly higher MD_{perc} ($F(2, 497) = 63.3$, $p < .001$, $R^2_{Adjusted} = .20$, effect = 0.0000067 mm^2/s). In the CAB, female subjects demonstrated significantly higher FA_{perc} ($F(2, 497) = 14.0$, $p < .001$, $R^2_{Adjusted} = .05$, effect = 0.011). In the UNC, male subjects demonstrated significantly higher FA_{perc} ($F(2, 497) = 3.1$, $p = .046$, $R^2_{Adjusted} = .008$, effect = 0.0063) (Figure 5).

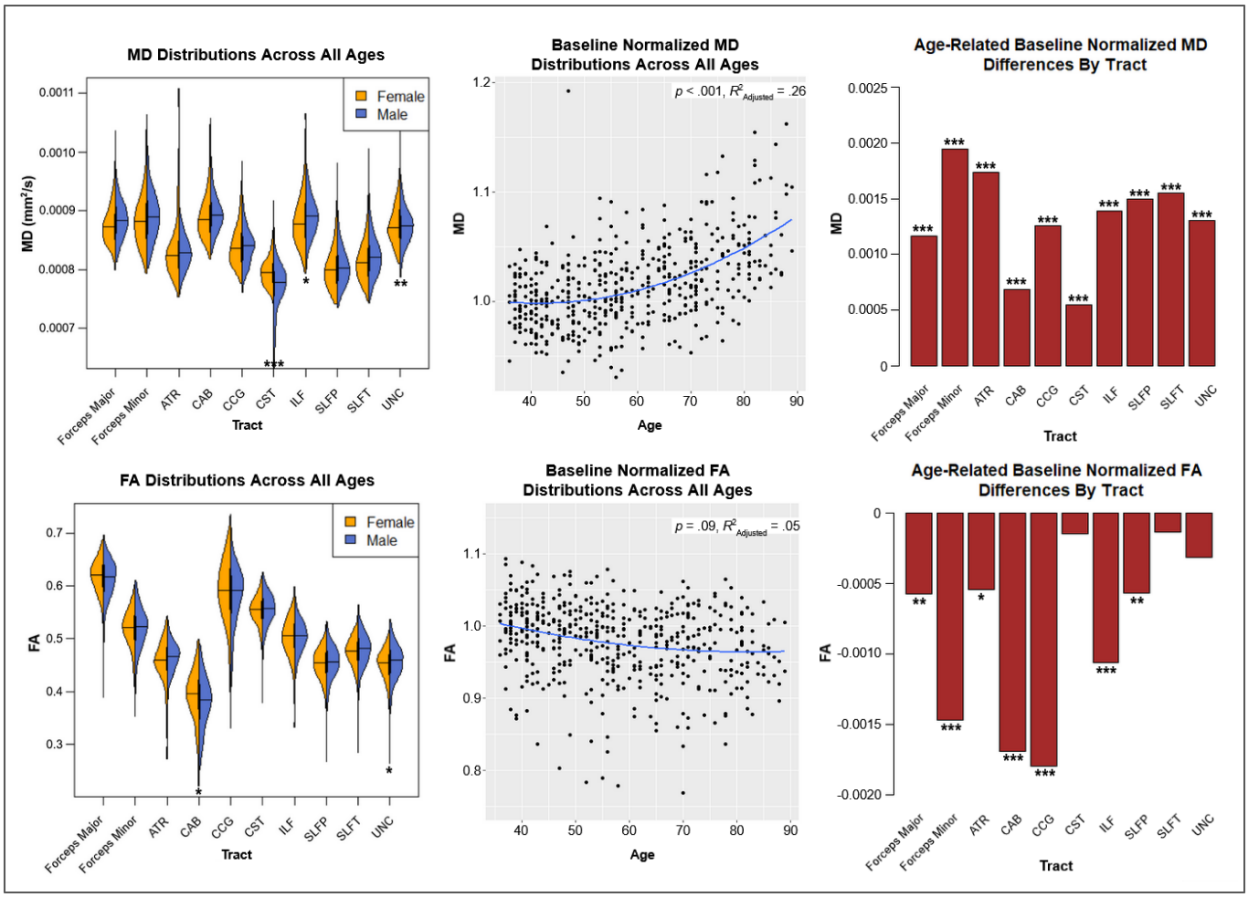

Figure 5: Raw MD and FA distributions separated by sex (left), whole-WM age effects on MD_{perc}, and FA_{perc} (middle), and tractwise age effects for MD_{perc}, and FA_{perc} (right).

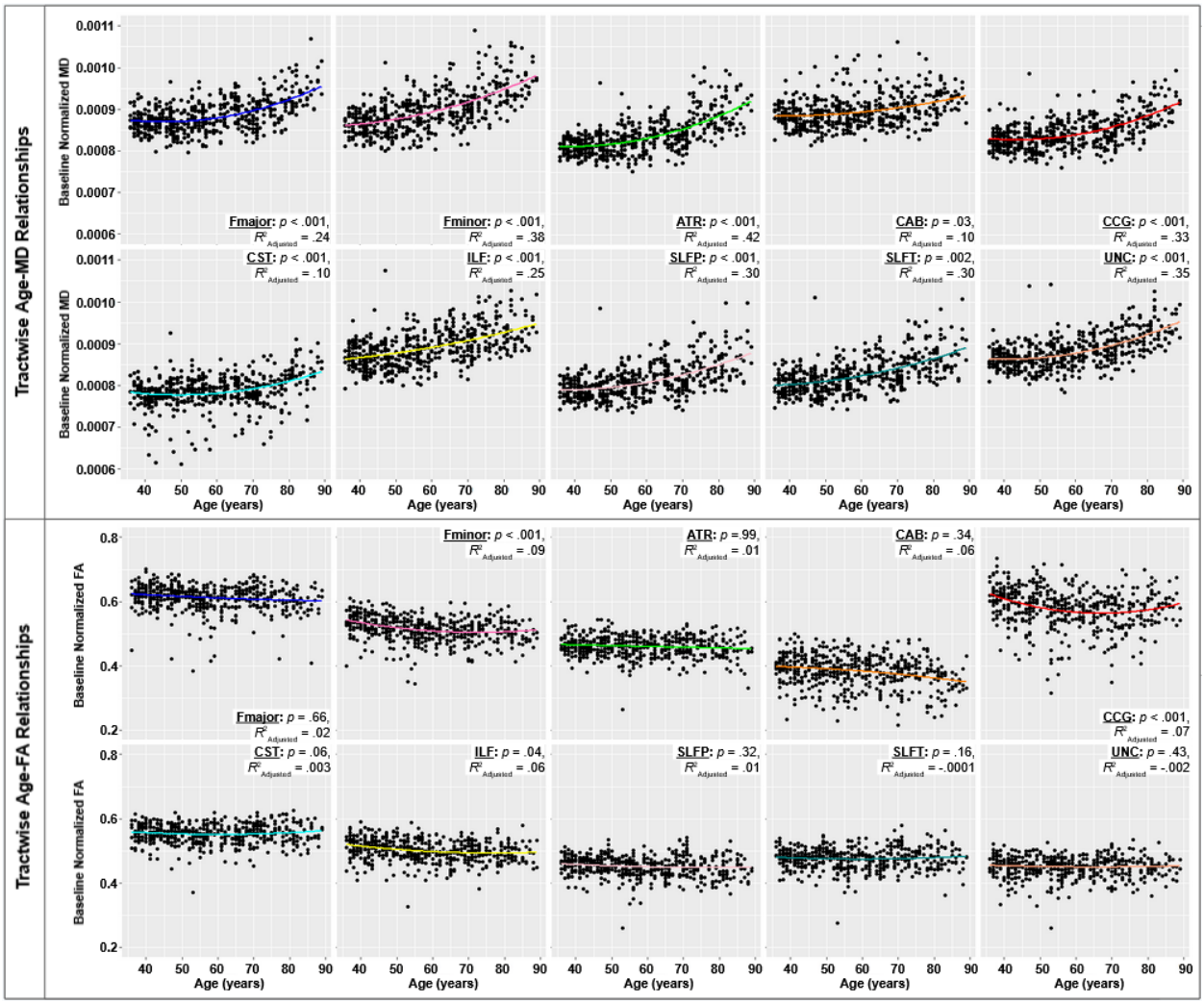

Figure 6: Tractwise quadratic regression of age effects on Length$_{perc}$ and Volume$_{perc}$

Whole-WM morphometry-Microstructure Relationships

Model 1 (morphometry vs. microstructure):

Mean tract Length$_{perc}$ was significantly negatively associated with MD$_{perc}$ ($F(2, 497) = 12.3$, $p < .001$, $R^2_{Adjusted} = .04$, effect = -0.21), and significantly positively associated with FA$_{perc}$ ($F(2, 497) = 8.1$, $p < .001$, $R^2_{Adjusted} = .03$, effect = 0.27). Mean tract VLR$_{perc}$ was significantly negatively associated with both MD$_{perc}$ ($F(2, 497) = 11.3$, $p < .001$, $R^2_{Adjusted} = .04$, effect = -0.049) and FA$_{perc}$ ($F(2, 497) = 8.4$, $p < .001$, $R^2_{Adjusted} = .03$, effect = -0.069) (Table 1a).

Length$_{perc}$ vs. MD$_{perc}$ and FA$_{perc}$: significant negative associations with MD$_{perc}$ were identified in Fminor, CST, SLFP and UNC. Significant positive associations with FA$_{perc}$ were identified in Fminor, ATR, CAB, CST, and ILF, and SLFT.

VLR_{perc} vs. MD_{perc} and FA_{perc}: significant negative associations with MD_{perc} were identified in the Fmajor, Fminor, ATR, CCG, SLFP, SLFT, and UNC, and a significant positive association in the CAB. Significant negative associations with FA_{perc} were identified in the Fmajor, ATR, CAB, CST, and UNC (Table 1b).

Model 2 (Sex differences in morphometry-microstructure relationships):

After dividing the sample by sex, a significant positive association was found between $Length_{perc}$ and FA_{perc} in the female sample ($F(2, 291) = 13.2$, $p < .001$, $R^2_{Adjusted} = .08$, effect = 0.26), while negative associations were identified between VLR_{perc} and FA_{perc} in both female ($F(2, 291) = 23.5$, $p < .001$, $R^2_{Adjusted} = .13$, effect = -0.13) and male ($F(2, 203) = 10.7$, $p < .001$, $R^2_{Adjusted} = .09$, effect = -0.11) subjects. No significant associations were identified between morphometry and MD_{perc} after dividing the sample by sex (Table 2a).

$Length_{perc}$ vs. MD_{perc} and FA_{perc}: a significant positive association with MD_{perc} was identified in female subjects in the ATR, while a significant negative association was found in the CST for male subjects. Female subjects demonstrated significant positive relationships between length and FA_{perc} in the ATR, CAB, CST, ILF, and SLFT, in addition to a significant negative association in the UNC, while male subjects demonstrated a significant negative association in the SLFP and a significant positive association in the ILF.

VLR_{perc} vs. MD_{perc} and FA_{perc}: both female and male subjects demonstrated significant positive associations between VLR and MD_{perc} in the CAB, with male subjects showing significant negative associations in the Fmajor and SLFT. Both sexes demonstrated significant negative associations between VLR and FA_{perc} in the Fmajor, Fminor, ATR, CAB, CST, and UNC, with Female subjects showing significant negative associations in the ILF. Female subjects showed an additional significant positive association with FA_{perc} in the SLFT (Table 2b).

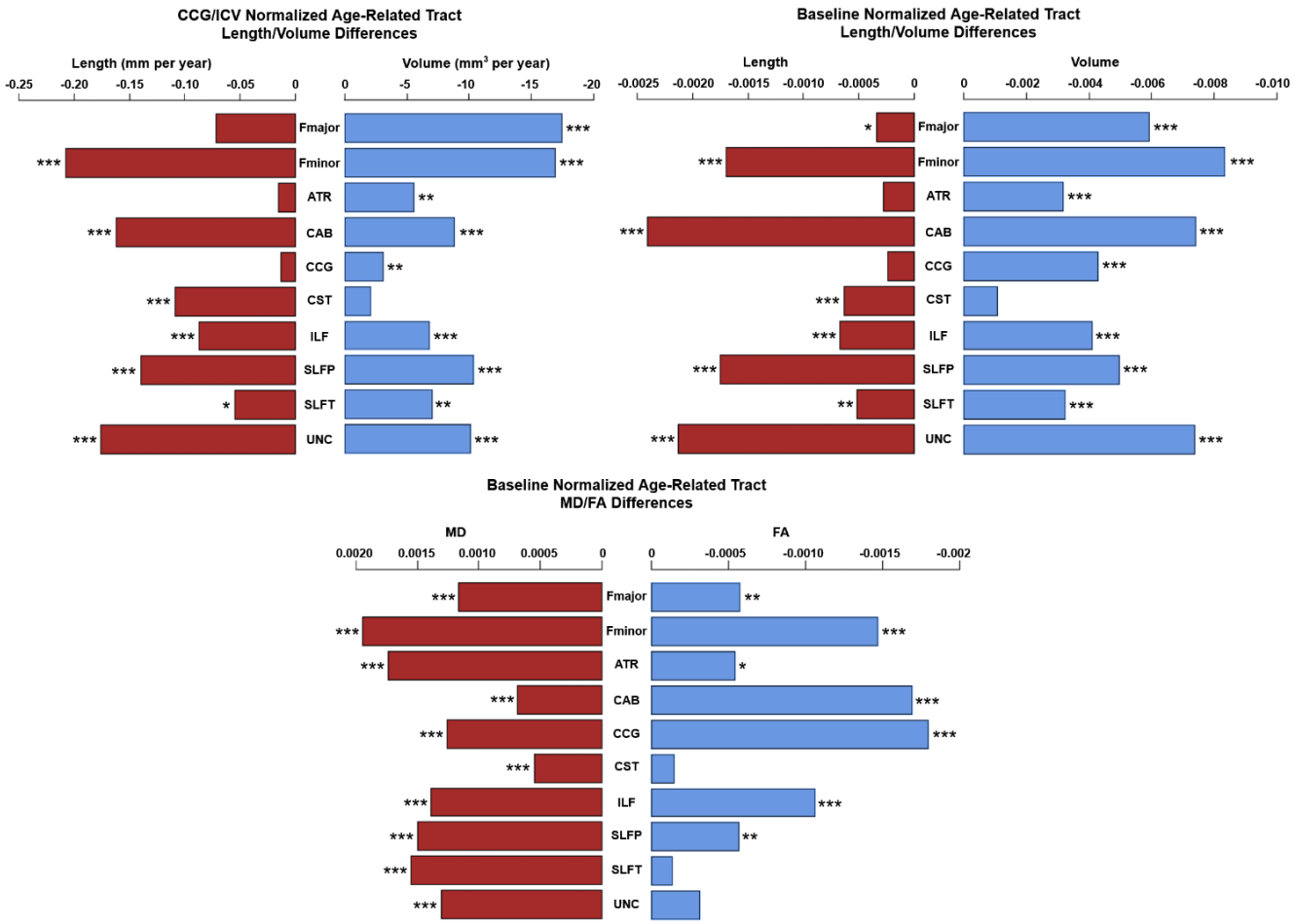

Figure 7: Tractwise age effects for $Length_{norm}$ and $Volume_{norm}$ (top left), $Length_{perc}$ and $Volume_{perc}$ (top right), and MD_{perc} and FA_{perc} (bottom)

Table 1a: Model 1 - Tractwise Length/VLR Relationships with Microstructure (Covaried for Sex).
Significant associations are bolded. Asterisks indicate significance (*:p<.05, **:p<.01, ***:p<.001).

	Baseline Normalized Length		**Baseline Normalized VLR**	
Tract	FA	MD	FA	MD
All	$F(2, 497) = 8.1$, $p < .001$, $R^2_{Adjusted} = .03$	$F(2, 497) = 12.3$, $p < .001$, $R^2_{Adjusted} = .04$	$F(2, 497) = 8.4$, $p < .001$, $R^2_{Adjusted} = .03$	$F(2, 497) = 11.3$, $p < .001$, $R^2_{Adjusted} = .04$
	0.2739* **	**-0.205382*** **	**-0.069165*** **	**-0.048962*** **

Table 1b: Model 1 - Tractwise Length/VLR Relationships with Microstructure (Covaried for Sex).
Significant associations are bolded. Asterisks indicate significance (*, **, ***).

	Baseline Normalized Length		**Baseline Normalized VLR**	
Tract	FA	MD	FA	MD
Fmajor	$F(2, 490) = 8.6$, $p < .001$, $R^2_{Adjusted} = .03$	$F(2, 490) = 5.5$, $p = .004$, $R^2_{Adjusted} = .02$	$F(2, 490) = 37.3$, $p < .001$, $R^2_{Adjusted} = .13$	$F(2, 490) = 22.1$, $p < .001$, $R^2_{Adjusted} = .08$
	-0.04608	0.035005	**-0.098857*** **	**-0.053311*** **
Fminor	$F(2, 490) = 18.6$, $p < .001$, $R^2_{Adjusted} = .07$	$F(2, 490) = 12.6$, $p < .001$, $R^2_{Adjusted} = .04$	$F(2, 490) = 4.0$, $p = .018$, $R^2_{Adjusted} = .01$	$F(2, 490) = 26.8$, $p < .001$, $R^2_{Adjusted} = .10$
	0.278180* **	**-0.193894*** **	-0.021944	**-0.094222*** **
ATR	$F(2, 494) = 8.14$, $p < .001$, $R^2_{Adjusted} = .03$	$F(2, 494) = 1.8$, $p = .17$, $R^2_{Adjusted} = .003$	$F(2, 494) = 3.9$, $p = .021$, $R^2_{Adjusted} = .001$	$F(2, 494) = 10.0$, $p < .001$, $R^2_{Adjusted} = .04$
	0.238199 **	0.066739	**-0.044185* **	**-0.051504*** **

CAB	$F(2, 487) = 11.9$, $p < .001$, $R^2_{Adjusted} = .04$	$F(2, 487) = 0.9$, $p = .41$, $R^2_{Adjusted} = -.0005$	$F(2, 487) = 39.7$, $p < .001$, $R^2_{Adjusted} = .14$	$F(2, 487) = 14.2$, $p < .001$, $R^2_{Adjusted} = .05$
	0.27627* **	-0.018313	**-0.181946*** **	**0.038189*** **
CCG	$F(2, 492) = 3.3$, $p = .04$, $R^2_{Adjusted} = .009$	$F(2, 492) = 1.1$, $p = .32$, $R^2_{Adjusted} = .0006$	$F(2, 492) = 2.7$, $p = .07$, $R^2_{Adjusted} = .006$	$F(2, 492) = 4.9$, $p = .008$, $R^2_{Adjusted} = .02$
	0.101756	-0.048128	-0.009779	**-0.026859** **
CST	$F(2, 488) = 16.7$, $p < .001$, $R^2_{Adjusted} = .06$	$F(2, 488) = 13.7$, $p < .001$, $R^2_{Adjusted} = .05$	$F(2, 488) = 9.8$, $p < .001$, $R^2_{Adjusted} = .03$	$F(2, 488) = 6.3$, $p = .002$, $R^2_{Adjusted} = .02$
	0.322350* **	**-0.185796*** **	**-0.083342*** **	-0.010078
ILF	$F(2, 494) = 16.2$, $p < .001$, $R^2_{Adjusted} = .06$	$F(2, 494) = 4.0$, $p = .02$, $R^2_{Adjusted} = .01$	$F(2, 494) = 4.4$, $p = .01$, $R^2_{Adjusted} = .01$	$F(2, 494) = 8.9$, $p < .001$, $R^2_{Adjusted} = .03$
	0.292647* **	-0.035711	-0.033044	**-0.03546** **
SLFP	$F(2, 494) = 2.0$, $p = .14$, $R^2_{Adjusted} = .004$	$F(2, 494) = 16.0$, $p < .001$, $R^2_{Adjusted} = .06$	$F(2, 494) = 3.4$, $p = .03$, $R^2_{Adjusted} = .01$	$F(2, 494) = 9.2$, $p < .001$, $R^2_{Adjusted} = .032$
	-0.02100	**-0.170268*** **	0.024718	**-0.038083*** **
SLFT	$F(2, 492) = 5.3$, $p = .005$, $R^2_{Adjusted} = .006$	$F(2, 492) = 1.0$, $p = .36$, $R^2_{Adjusted} = .0001$	$F(2, 492) = 5.5$, $p = .004$, $R^2_{Adjusted} = .02$	$F(2, 492) = 5.7$, $p = .004$, $R^2_{Adjusted} = .02$
	**0.113639* **	0.0003681	0.034896	**-0.0338737** **
UNC	$F(2, 492) = 5.7$, $p = .004$, $R^2_{Adjusted} = .004$	$F(2, 492) = 3.9$, $p = .02$, $R^2_{Adjusted} = .01$	$F(2, 492) = 15.8$, $p < .001$, $R^2_{Adjusted} = .06$	$F(2, 492) = 13.7$, $p < .001$, $R^2_{Adjusted} = .05$
	-0.070574	**-0.0582656** **	**-0.094532* **	**-0.058137*** **

Table 2a: Model 2 - Tractwise Sex Differences Relationships Between Length/VLR and Microstructure (Covaried for Age). Significant associations are bolded. Asterisks indicate significance (*:p<.05, **:p<.01, ***:p<.001).

	Baseline Normalized Length				**Baseline Normalized VLR**			
	FA		MD		FA		MD	
Tract	Female	Male	Female	Male	Female	Male	Female	Male
All	$F(2, 291) = 13.2$, $p < .001$, $R^2_{Adjusted} = .08$	$F(2, 203) = 1.7$, $p = .19$, $R^2_{Adjusted} = .006$	$F(2, 291) = 55.0$, $p < .001$, $R^2_{Adjusted} = .27$	$F(2, 203) = 23.3$, $p < .001$, $R^2_{Adjusted} = .18$	$F(2, 291) = 23.5$, $p < .001$, $R^2_{Adjusted} = .13$	$F(2, 203) = 10.7$, $p < .001$, $R^2_{Adjusted} = .09$	$F(2, 291) = 55.2$, $p < .001$, $R^2_{Adjusted} = .27$	$F(2, 203) = 23.3$, $p < .001$, $R^2_{Adjusted} = .18$
	0.2642212**	0.0860415	0.0173169	-0.0825040	**-0.1276850*****	**-0.1078291*****	0.0091113	-0.0128556

Table 2b: Model 2 - Tractwise Sex Differences Relationships Between Length/VLR and Microstructure (Covaried for Age). Significant associations are bolded. Asterisks indicate significance (*:p<.05, **:p<.01, ***:p<.001).

	Baseline Normalized Length				**Baseline Normalized VLR**			
	FA		MD		FA		MD	
Tract	Female	Male	Female	Male	Female	Male	Female	Male
Fmajor	$F(2, 287) = 3.8$, $p = .02$, $R^2_{Adjusted} = .02$	$F(2, 200) = 2.0$, $p = .14$, $R^2_{Adjusted} = .01$	$F(2, 287) = 32.6$, $p < .001$, $R^2_{Adjusted} = .18$	$F(2, 200) = 8.7$, $p < .001$, $R^2_{Adjusted} = .07$	$F(2, 287) = 32.8$, $p < .001$, $R^2_{Adjusted} = .18$	$F(2, 200) = 18.9$, $p < .001$, $R^2_{Adjusted} = .15$	$F(2, 287) = 33.3$, $p < .001$, $R^2_{Adjusted} = .18$	$F(2, 200) = 12.5$, $p < .001$, $R^2_{Adjusted} = .10$
	-0.0828130	-0.0250057	0.060691	0.0400270	**-0.1423231*****	**-0.113219*****	-0.0255641	**-0.0363143***
Fminor	$F(2, 288) = 24.1$, $p < .001$, $R^2_{Adjusted} = .14$	$F(2, 199) = 12.3$, $p <$	$F(2, 288) = 76.8$, $p <$	$F(2, 199) = 26.8$, $p <$	$F(2, 288) = 28.0$, $p < .001$, $R^2_{Adjusted} = .16$	$F(2, 199) = 32.1$, $p < .001$, $R^2_{Adjusted} = .24$	$F(2, 288) = 78.6$, $p < .001$, $R^2_{Adjusted} = .35$	$F(2, 199) = 26.6$, $p < .001$, $R^2_{Adjusted} = .20$

		.001, $R^2_{Adjusted}$ = .10	.001, $R^2_{Adjusted}$ = .34	.001, $R^2_{Adjusted}$ = .20				
	0.1248283	0.159234	0.0283315	-0.026312	**-0.0767406****	**-0.1788177*****	-0.0279077	-0.0003307
ATR	$F(2, 289) = 10.7$, $p < .001$, $R^2_{Adjusted} = .06$	$F(2, 202) = 2.3$, $p = .11$, $R^2_{Adjusted} = .01$	$F(2, 289) = 70.9$, $p < .001$, $R^2_{Adjusted} = .32$	$F(2, 202) = 32.4$, $p < .001$, $R^2_{Adjusted} = .24$	$F(2, 289) = 8.0$, $p < .001$, $R^2_{Adjusted} = .05$	$F(2, 202) = 3.0$, $p = .05$, $R^2_{Adjusted} = .02$	$F(2, 289) = 66.6$, $p < .001$, $R^2_{Adjusted} = .31$	$F(2, 202) = 32.3$, $p < .001$, $R^2_{Adjusted} = .23$
	0.2639673**	0.1871177	**0.1661641****	0.0270416	**-0.0520953***	**-0.0643893***	-0.0304697	0.0057680
CAB	$F(2, 285) = 11.9$ $p < .001$, $R^2_{Adjusted} = .07$	$F(2, 199) = 5.3$, $p = .006$, $R^2_{Adjusted} = .04$	$F(2, 285) = 14.1$, $p < .001$, $R^2_{Adjusted} = .08$	$F(2, 199) = 2.2$, $p = .11$, $R^2_{Adjusted} = .01$	$F(2, 285) = 40.9$, $p < .001$, $R^2_{Adjusted} = .22$	$F(2, 199) = 32.5$, $p < .001$, $R^2_{Adjusted} = .24$	$F(2, 285) = 26.4$, $p < .001$, $R^2_{Adjusted} = .15$	$F(2, 199) = 14.6$, $p < .001$, $R^2_{Adjusted} = .12$
	0.2272627*	0.168635	0.0337673	0.0091595	**-0.2208762*****	**-0.2198324*****	**0.0529135*****	**0.0451134*****
CCG	$F(2, 289) = 15.1$, $p < .001$, $R^2_{Adjusted} = .09$	$F(2, 200) = 4.8$, $p = .009$, $R^2_{Adjusted} = .04$	$F(2, 289) = 40.1$, $p < .001$, $R^2_{Adjusted} = .21$	$F(2, 200) = 19.2$, $p < .001$, $R^2_{Adjusted} = .15$	$F(2, 289) = 16.2$, $p < .001$, $R^2_{Adjusted} = .09$	$F(2, 200) = 5.8$, $p = .004$, $R^2_{Adjusted} = .04$	$F(2, 289) = 40.7$, $p < .001$, $R^2_{Adjusted} = .21$	$F(2, 200) = 18.4$, $p < .001$, $R^2_{Adjusted} = .15$
	0.0864906	0.0558766	-0.0126488	-0.0528734	-0.0445464	-0.0458499	-0.0117917	0.0047262
CST	$F(2, 284) = 19.6$, $p < .001$, $R^2_{Adjusted} = .12$	$F(2, 201) = 1.6$, $p = .20$, $R^2_{Adjusted} = .006$	$F(2, 284) = 11.4$, $p < .001$, $R^2_{Adjusted} = .07$	$F(2, 201) = 3.9$, $p = .02$, $R^2_{Adjusted} = .03$	$F(2, 284) = 8.3$, $p < .001$, $R^2_{Adjusted} = .05$	$F(2, 201) = 2.8$, $p = .06$, $R^2_{Adjusted} = .02$	$F(2, 284) = 9.6$, $p < .001$, $R^2_{Adjusted} = .06$	$F(2, 201) = 1.8$, $p = .16$, $R^2_{Adjusted} = .008$
	0.4511***	0.1562529	-0.1060181	**-0.2127942***	**-0.0912455*****	**-0.07439***	0.0156612	-0.0361108

ILF	$F(2, 289) = 17.5$, $p < .001$, $R^2_{Adjusted} = .10$	$F(2, 202) = 6.6$, $p = .002$, $R^2_{Adjusted} = .05$	$F(2, 289) = 42.6$, $p < .001$, $R^2_{Adjusted} = .22$	$F(2, 202) = 17.7$, $p < .001$, $R^2_{Adjusted} = .14$	$F(2, 289) = 17.4$, $p < .001$, $R^2_{Adjusted} = .10$	$F(2, 202) = 5.3$, $p = .006$, $R^2_{Adjusted} = .04$	$F(2, 289) = 42.0$, $p < .001$, $R^2_{Adjusted} = .23$	$F(2, 202) = 18.2$, $p < .001$, $R^2_{Adjusted} = .14$
	0.2739332**	**0.2020411***	0.0554729	0.0199349	**-0.0777284*****	-0.0458436	0.0078882	-0.0151325
SLFP	$F(2, 288) = 7.6$, $p < .001$, $R^2_{Adjusted} = .04$	$F(2, 203) = 2.6$, $p = .07$, $R^2_{Adjusted} = .02$	$F(2, 288) = 48.1$, $p < .001$, $R^2_{Adjusted} = .25$	$F(2, 203) = 21.8$, $p < .001$, $R^2_{Adjusted} = .17$	$F(2, 288) = 9.1$, $p < .001$, $R^2_{Adjusted} = .05$	$F(2, 203) = 0.04$, $p = .96$, $R^2_{Adjusted} = -.009$	$F(2, 288) = 47.6$, $p < .001$, $R^2_{Adjusted} = .24$	$F(2, 203) = 23.2$, $p < .001$, $R^2_{Adjusted} = .18$
	0.0133190	**-0.1783119***	-0.0410698	-0.0632879	0.0322023	0.0031588	-0.002180	-0.027266
SLFT	$F(2, 287) = 6.8$, $p = .001$, $R^2_{Adjusted} = .04$	$F(2, 202) = 2.1$, $p = .12$, $R^2_{Adjusted} = .01$	$F(2, 287) = 53.4$, $p < .001$, $R^2_{Adjusted} = .27$	$F(2, 202) = 23.0$, $p < .001$, $R^2_{Adjusted} = .18$	$F(2, 287) = 7.0$, $p = .001$, $R^2_{Adjusted} = .04$	$F(2, 202) = 2.6$, $p = .07$, $R^2_{Adjusted} = .02$	$F(2, 287) = 52.7$, $p < .001$, $R^2_{Adjusted} = .26$	$F(2, 202) = 26.8$, $p < .001$, $R^2_{Adjusted} = .20$
	0.1452281*	0.0674176	0.0546752	0.0559634	**0.0472768***	0.0297067	0.009540	**-0.0377372***
UNC	$F(2, 290) = 3.8$, $p = .02$, $R^2_{Adjusted} = .02$	$F(2, 199) = 1.2$, $p = .30$, $R^2_{Adjusted} = .002$	$F(2, 290) = 50.0$, $p < .001$, $R^2_{Adjusted} = .25$	$F(2, 199) = 18.9$, $p < .001$, $R^2_{Adjusted} = .15$	$F(2, 290) = 18.8$, $p < .001$, $R^2_{Adjusted} = .11$	$F(2, 199) = 5.1$, $p = .007$, $R^2_{Adjusted} = .04$	$F(2, 290) = 40.4$, $p < .001$, $R^2_{Adjusted} = .25$	$F(2, 199) = 20.4$, $p < .001$, $R^2_{Adjusted} = .16$
	-0.1322017*	-0.0744272	0.0235803	0.0242088	**-0.1762967*****	**-0.0994434****	0.0188674	-0.0295714

Tractwise canonical correlations

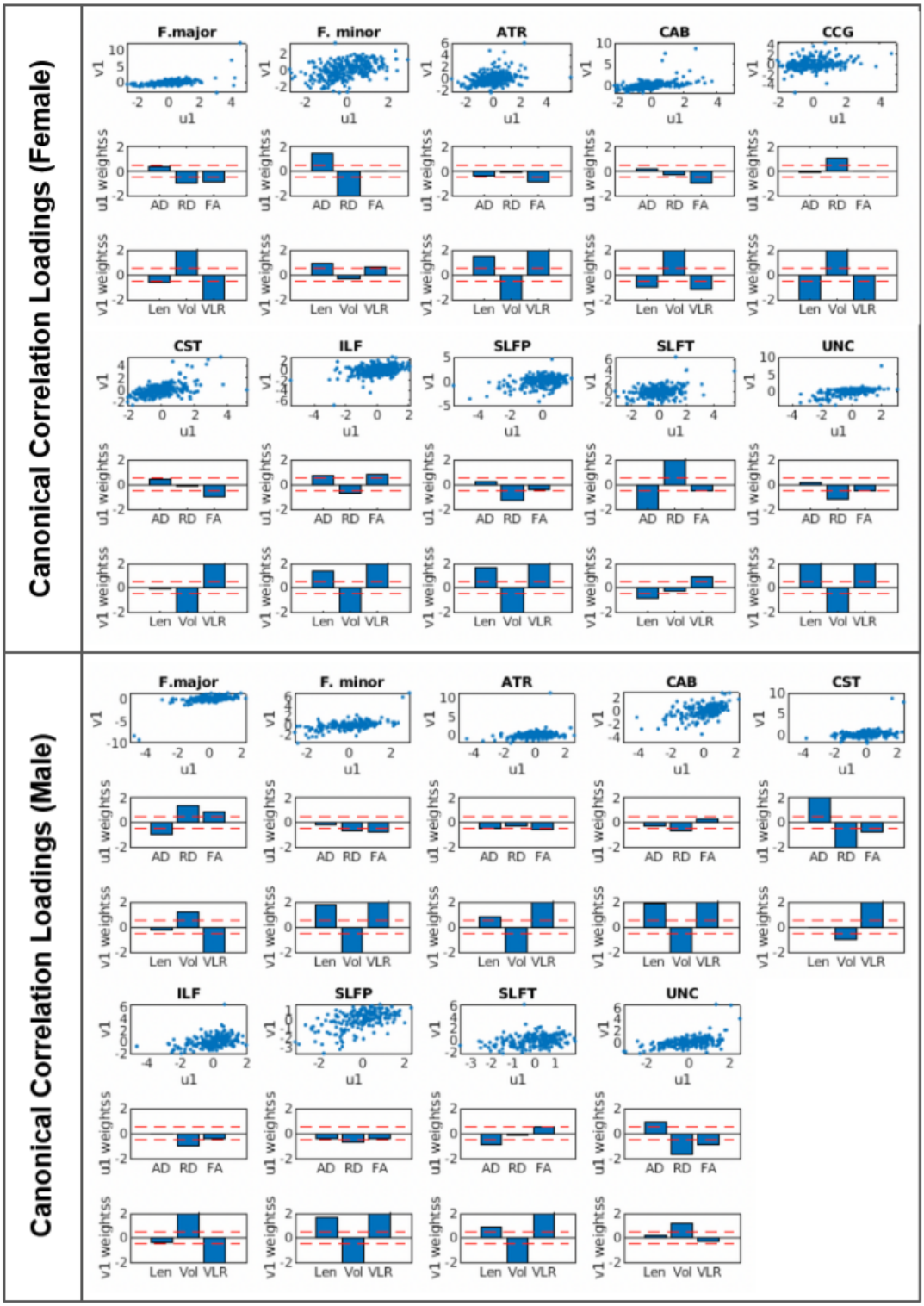

Figure 8: Tractwise contributions by microstructural (AD_{perc}/RD_{perc}/FA_{perc}) and morphometric ($Length_{perc}$/$Volume_{perc}$/VLR_{perc}) measures to categorical perfusion-microstructure relationships separated by sex.

CCA analysis identified varying patterns of tractwise microstructural and morphometric loadings between male and female subjects (Figure 8). Loadings are listed only for statistically significant canonical correlations, and all loadings are thresholded at 0.5. CCA findings are categorized into “morphometric”, “microstructural” and “morphometic-microstructural”, as shown in Table 3 along with their likely interpretations. Notably, the most common morphometric pattern is (i), implying prolonged survival of the largest fibres. Sex-independent common morphometric relationships include opposite loadings in length and volume in the ATR, CAB, and SLFT, and volume loading without significant length loading in the CST. Regarding microstructural findings, both males and females exhibit relationship (iv) in the UNC and pattern (vi) in the ATR, implying degeneration of crossing fibres in these tracts. Both sexes also exhibit pattern (vii) in the SLFP, suggesting negligible cross-fibre contribution. The morphometric-microstructural patterns displayed no commonality between sexes.

Males exhibit pattern (ii) in 3 additional tracts than females (i.e. Fmajor, ILF, UNC), implying less participation of secondary fibre degeneration in the morphometric loss. Females display pattern (vii) in anterior-superior WM (i.e. Fminor, CCG), a sign of negligible cross-fibre contribution, whereas males display pattern (vii) in lateral-inferior tracts (i.e. CAB, ILF). Females exhibit more significant microstructural-morphometric loading patterns than males. Females exhibit pattern (viii) in the Fminor and SLFP, implicating loss of tract length and packing density, consistent with their display of pattern (iii); males do not. Instead, males exhibit pattern (ix) in the Fmajor, also associated with loss of packing density. Males alone exhibit pattern (x) in the UNC, associated with more advanced degeneration.

Category	**Pattern**	**Likely interpretation**	**Implicated tracts**
Morphometric	**(i) Len and vol loading opposite**	The largest fibres surviving longest, intermediate degeneration	F(ATR, CAB, SLFP, Fmajor, ILF, UNC, CCG) M(ATR, CAB, SLFP, Fminor, SLFT)
	(ii) Vol loading with negligible len	Fibers degenerate evenly, regardless of size	F(CST) M(CST, Fmajor, ILF, UNC)
	(iii) Len loading with negligible vol	Fibre degeneration driven by loss in length and fibre packing density	F(Fminor, SLFT)
Microstructural	**(iv) RD and FA loading coincide**	Selective degeneration of crossing fibres - secondary fibres degenerate more	F(UNC, Fmajor) M(UNC, Fminor, CST)
	(v) RD and FA loadings opposite	Negligible selective degeneration of crossing fibres	F(SLFT)
	(vi) FA loading with negligible RD	Crossing fibre contribution -	F(ATR, CAB, CST)

		demyelination with obstruction of axial diffusivity**, or** primary fibre contribution - obstruction of axial diffusivity with minimal demyelination	M(ATR, SLFT)
	(vii) RD loading with negligible FA	Selective degeneration of crossing fibres - secondary fibres degenerate more	F(SLFP, Fminor, CCG) M(SLFP, CAB, ILF)
Morphometric-microstructural	**(viii) Len and RD loadings opposite**	Loss in length co-exists with rise in extracellular space, implicating loss of packing density	F(Fminor, SLFT)
	(ix) Vol and RD loadings together	Volume is higher in the presence of loss of packing density driven by increase in extracellular space	M(Fmajor)
	(x) Vol and RD loadings opposite	Loss in volume co-exists with rise in extracellular space, more advanced degeneration	F(Fmajor) M(UNC)

Table 3: Histological interpretations of morphometry-microstructure relationships identified by CCA analysis

Tractwise cross-correlations

At zero lag, significant correlations between $Length_{perc}$ and FA_{perc} were identified in the Fminor, and SLFP, between $Length_{perc}$ and AD_{perc} in the Fminor, ATR, CAB, CCG, ILF, and SLFP, and between $Length_{perc}$ and RD_{perc} in the Fminor, ATR, CAB, CCG, ILF, and SLFP. A single correlation at negative lag was identified between $Length_{perc}$ and FA_{perc} in the CCG, in which $Length_{pert}$ led FA_{perc} by approximately seven years. No significant tractwise correlations were identified between $Volume_{perc}$ and our microstructural variables.

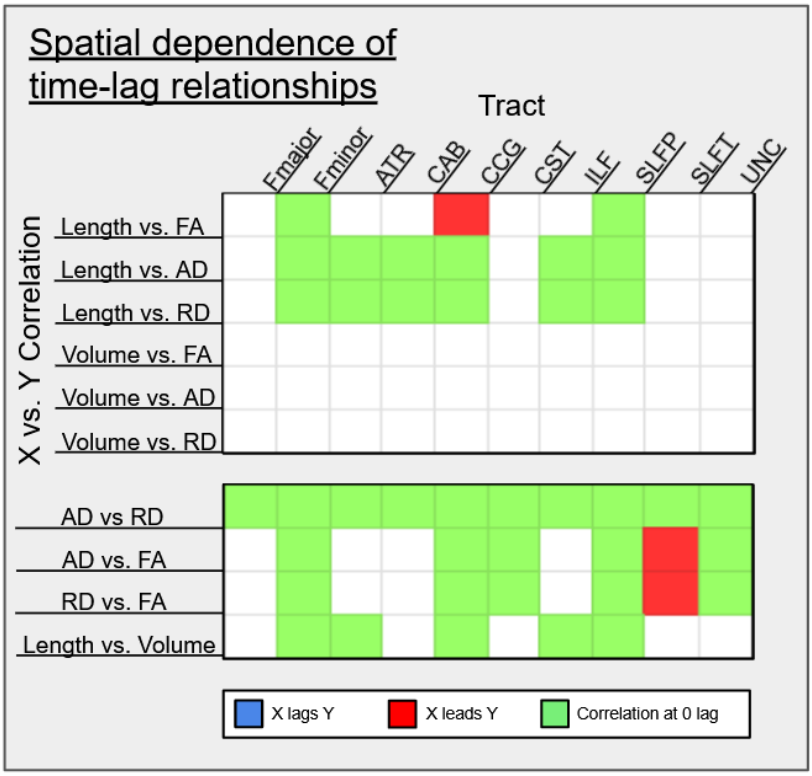

Figure 9: Tractwise cross-correlation results demonstrating significant correlations at positive, negative and zero lag by age category.

Comparing $Length_{perc}$ to $Volume_{perc}$ found significant correlations at 0 lag in the Fminor, ATR, CCG, ILF, and SLFP. All tracts demonstrated significant 0 lag correlations between AD_{perc} and RD_{perc}. Significant correlations between both AD_{perc} and FA_{perc}, as well as AD_{perc} and FA_{perc}, were identified at 0 lag in the Fminor, CCG, CST, SLFP, and UNC, along with correlations at negative lag in the SLFT, in which AD_{perc} led FA_{perc} by approximately fourteen years. (Figure 9)

DISCUSSION

Our initial hypotheses posited that (1) age-related microstructural differences would be greater in tracts that demonstrate greater age-related morphometrical differences, and (2) tracts that become relatively thinner with age will have relatively high mean tract lengths. While consistent trends in morphometric and microstructural declines with age were identified in the majority of tracts, tractwise relationships between morphometry and microstructure were demonstrated to be highly variable across

the brain, as well as between sexes, rather than following consistent patterns across tracts per our hypotheses.

Age and morphometry:

We started our analyses with raw (unnormalized) tract volume and length, and in line with existing research on white matter atrophy (de Groot et al., 2015; Sala et al., 2012; Tang et al., 1997), we observed associations between advancing age and overall decreases in both raw tract volume and raw tract length. Raw VLR, as a surrogate of fibre thickness, also decreases in the majority of regions of interest, demonstrating that tracts typically become thinner with age. At the tractwise level, decreasing raw tract volume in aging was found in all tested tracts with the exception of the CST. Conversely to the CST, the forceps major and forceps minor exhibited notably greater age-related raw volume differences than other WM regions. All tracts except three (forceps major, ATR, and CCG) also shortened in aging (Figure X). The CCG, due to the observed age stability in its length, recommended itself as the normalization target in subsequent tract length analyses. When length and volume were both normalized (volume by ICV and length by CCG length), the $length_{perc}$ and $volume_{perc}$ decreases in WM overall still outpaced those in the reference structure.

Taken together, our findings demonstrate that $length_{perc}$ and $volume_{perc}$ do not decline proportionately in aging. Tracts like the CST do in fact shorten with age without significant corresponding losses in $volume_{perc}$. In contrast, tracts like the CCG would be expected to demonstrate the opposite pattern, narrowing with age as it loses $volume_{perc}$ with relatively little loss in tract $length_{perc}$. Another interpretation is that tractwise morphometric variability represents a cross-sectional observation of stages in an ongoing, but shared trajectory of decline. This would suggest that the pattern of morphometric decline is common across the brain, but takes effect at different ages or rates between tracts due to regionally specific protective or exacerbating factors. In either case, the presence of underlying factors affecting differentiating tract trajectories of decline requires clarification.

Age and microstructure:

Relationships between age and WM integrity across tracts note the expected trends of increasing MD_{perc} and decreasing FA_{perc} with advancing age. This mirrors general findings in the literature regarding microstructural WM decline (Benitez et al., 2018; Sala et al., 2012). As in morphometric age associations, tracts varied considerably in their trajectory of microstructural changes. While all tracts demonstrated increases in MD, three tracts, the CST, SLFT, and UNC, exhibited no significant effects of age on FA_{perc}. This continues the trend observed in the morphometric data, in which the CST shows considerable robustness to aging declines. As both the SLFT and UNC are relatively posterior tracts, these findings

may be interpretable as support for retrogenesis theories on brain aging, however, significant MD_{perc} increases with age were nonetheless identified in all three tracts. Moreover, the UNC showed strong age effects on morphometry in both $length_{perc}$ and $volume_{perc}$. While microstructural age effects provide insight into the variation in declines across the brain, they also demonstrate the need to examine relationships between morphometry and microstructure to further clarify the basis of tractwise differences.

The morphometry-microstructure relationship: variations with age

Whole-WM trends from Model 1 suggest that higher MD_{perc} and lower FA_{perc} values were associated with lower mean tract $length_{perc}$ and lower white-WM $volume_{perc}$. However, these patterns were complicated by tractwise and sex differences observed in model 2, necessitating our examination of morphometry-microstructure contributions using canonical correlation (CCA).

Variation in both relative tract $volume_{perc}$ and $length_{perc}$ are assumed to be the result of age-related culling of axonal fibers, as noted in histological examination of the WM across age (Choy et al., 2020; Marner et al., 2003). Our results demonstrate that these values do not, however, decline together at the same rates across the brain. Variation in WM $volume_{perc}$ across age is present regardless of changes in tract $length_{perc}$, meaning that some tracts show relatively preserved $volume_{perc}$ despite notable losses in tract $length_{perc}$. This is theorized to be the result of variation in extracellular space at different stages of WM decline. Increased size of surviving fibres, as well as thickening of myelin in aging axons, results in notably larger mean diameter in the aging tract (Tang et al., 1997). The geometry of packing larger fibres produces an increase in extracellular space between the fibres and relatively lower impact on tract volume. This is in contrast to even degeneration of both large and small fibers, which could allow a more densely packed bundle and produces relatively greater losses in tract volume (Marner et al., 2003; Tang et al., 1997).

The CCG and CST represent notable outliers in the tracts of interest addressed by this study. The CST is both one of the first recognizable tracts in early brain development and one of the first to myelinate (Grotheer et al., 2022; H. Huang et al., 2009). In our study, it was also the only tract to not demonstrate changes in $volume_{perc}$, VLR_{perc} and FA_{perc} in aging, suggesting a considerable resilience to both macro- and micro-structural declines. In contrast, the CCG exhibited the strongest age associations with FA_{perc} as well as robust age effects on both tract $volume_{perc}$ and VLR_{perc}, but no age effects on tract $length_{perc}$. It was also the only tract to demonstrate an age-lagged correlation between morphometric and microstructural differences across age, with $length_{perc}$ differences leading FA_{perc} differences by more than a decade. These two tracts are thus strong candidates for more targeted investigation into the mechanisms of interaction between morphometry and microstructural integrity as they differ across regions.

The morphometry-microstructure relationship: variations by tract may be driven by sex differences

Results from Models 1 and 2 indicate that the micro-macrostructural associations are influenced by age and sex in a tract-specific manner, which was further clarified by the CCA results.

	Female	**Male**
Fmajor	Prolonged survival of largest fibres with maintained packing density. Selective degeneration of crossing fibres.	Even degeneration by fiber size with maintained packing density, with rise in extracellular space
Fminor	Prolonged survival of largest fibres with loss of packing density. Selective degeneration of crossing fibres.	Prolonged survival of largest fibres with maintained fiber density. Selective degeneration of crossing fibres.
ATR	Prolonged survival of largest fibres with maintained packing density. Crossing fiber demyelination with AD obstruction.	Prolonged survival of largest fibres with maintained packing density. Crossing fiber demyelination with AD obstruction.
CAB	Prolonged survival of largest fibres with maintained packing density. Crossing fiber demyelination with AD obstruction.	Prolonged survival of largest fibres with maintained packing density. Selective degeneration of crossing fibres.
CCG	Prolonged survival of largest fibres with maintained packing density. Selective degeneration of crossing fibres.	No association between morphometry and microstructure.
CST	Even degeneration by fiber size with maintained packing density. Crossing fiber demyelination with AD obstruction.	Even degeneration by fiber size with maintained packing density. Selective degeneration of crossing fibres.
ILF	Prolonged survival of largest fibres with maintained packing density. Negligible crossing fiber degeneration.	Even degeneration by fiber size with maintained packing density. Selective degeneration of crossing fibres.
SLFP	Prolonged survival of largest fibres with maintained packing density. Selective degeneration of crossing fibres.	Prolonged survival of largest fibres with maintained packing density. Selective degeneration of crossing fibres.
SLFT	Prolonged survival of largest fibres with loss of packing density. Negligible crossing fiber degeneration.	Prolonged survival of largest fibres with maintained packing density. Crossing fiber demyelination with AD obstruction.
UNC	Prolonged survival of largest fibres with loss of packing density. Selective degeneration of crossing fibres.	Even degeneration by fiber size with maintained packing density. Selective degeneration of crossing fibres.

Table 4: Proposed mechanisms of degeneration identified in each tract of interest based on results from CCA analysis. (Taha et al., 2022; Uddin et al., 2019)

The fusion of morphometric and microstructural observations in CCA allows us to examine regional differences in WM aging in view of the expected sex differences. For each combination, we have provided a likely interpretation based on known literature, as summarized in Table 4. The predominance of fibers demonstrating opposing loading in $\text{length}_{\text{perc}}$ and $\text{volume}_{\text{perc}}$ support our study's initial hypothesis that the culling of vulnerable axon fibers would result in proportionally longer surviving fibers (pattern (i)

in the CCA results), with the ATR, CAB, and SLFP demonstrating this pattern in both male and female subjects, as well as the Fmajor, CCG, ILF, and UNC in females and Fminor and SLFT in males. Conversely, preferential culling of shorter fibers in relatively posterior tracts (Fminor and SLFT), which lose a greater degree of fiber density rather than fiber $volume_{perc}$ may represent an intermediate step of decline in which the preferential die-off of shorter fibers has begun, but the tract $volume_{perc}$ has not yet compressed. (Figure X)

Commonalities across sexes

A higher degree of variation was observed in patterns of microstructural contributions to WM decline compared to those of morphometry. The CST was notable as the one tract in which relatively preserved $length_{perc}$ was observed in both sexes (pattern (ii)). Other notable commonalities were the UNC, ATR, and SLFP. In the UNC, both male and female subjects demonstrated contributions to microstructural decline by both FA_{perc} and RD_{perc}, with both metrics trending together. Relatively lower RD_{perc} in the presence of lower FA_{perc} suggests contributions by crossing fibers affecting local measures of RD_{perc}. A similar argument can be made for commonalities in the ATR between sexes, in which degradation of crossing fibers obstructs diffusivity along the fibers of the tract in question. This could result in FA_{perc} changes despite negligible changes in RD_{perc}. Conversely, both male and female subjects displayed contributions by RD_{perc} to microstructural declines in the absence of significant FA loading. In theory, this could indicate that the majority of change in these regions is due to degradation of the tract itself, rather than contributions from crossing fibers.

Sex differences

Our results further suggest sex differences in degree of protection or susceptibility to axonal culling, with microstructural declines in the Fmajor, Fminor, CAB, CST, ILF, and SLFT differed between sexes. As pattern (ii) was more common in males, extending as well to the Fmajor, ILF, and UNC, males may demonstrate less aging-related culling in these regions. In male subjects, cross-fiber degeneration also appears more prevalent in the Fminor and CST, compared to higher prevalence in the Fmajor in female subjects. This may be interpretable as a greater degree of degradation in posterior regions in male subjects, compared to greater prefrontal declines in female subjects. However,this degeneration appears to be contributed by crossing fibers, rather than the tracts in question. Female subjects also demonstrated patterns of RD_{perc} and FA_{perc} assumed to indicate lower contributions by crossing fibers to degradation in the SLFT, compared to higher crossing fiber contributions in the male SLFT, degradation of fibers associated with the SLFT may be a determining influence to differences in diffusion measures in the posterior white matter. Negligible degeneration from crossing fibers was noted in the female Fminor and CCG, along with the male CAB and ILF. This seems to suggest a fronto-parietal vs temporo-parietal

difference between sexes, with these regions showing more advanced declines in female and male subjects respectively.

Tractwise differences by sex extended to morphometric and microstructural contributions to WM decline. Loss of fiber $length_{perc}$ accompanied by relatively higher RD_{perc} were more common in female subjects, specifically in the Fminor and SLFT. This suggests more advanced overall degradation in these regions, corroborating the assumption that negligible contributions by crossing fibers in those tracts indicated greater degradation in the tracts in question. However, advanced degradation was also suggested by opposing trends in RD_{perc} and $volume_{perc}$ in the female Fmajor, along with the male UNC. Cumulatively, this seems to indicate the presence of additional variables determining whether advanced degradation contributes primarily to changes in $length_{perc}$ or changes in $volume_{perc}$. In the male Fmajor, relatively higher $volume_{perc}$ in the presence of increasing RD_{perc} suggests loss of axonal packing density and an increase in extracellular space that may be similarly contributing to morphometric distinctions in other regions.

Across tracts, male subjects demonstrate a higher rate of even fiber degeneration by size, notably in the male Fmajor, CST, ILF, and UNC. This is in contrast to the biased degeneration of smaller fibers found more uniformly across tracts in the female subjects. The one exception in the female sample was the CST. The CST has both shown a higher mean fiber diameter (S. Y. Huang et al., 2020), and been observed to survive relatively intact across the lifespan (de Groot et al., 2016; Yeatman et al., 2014), this suggests that the even fiber degeneration in male subjects represents a less advanced stage of WM decline. Even degeneration of both smaller and larger fibers appears then to precede the biased degeneration seen in more advanced stages of decline that results in a predominance of longer surviving axonal fibers and a higher mean tract $length_{perc}$. (Choy et al., 2020; Marner et al., 2003; Tang et al., 1997). Differences in signatures of decline could then reflect differences in range of fiber length, as $length_{perc}$ changes in tracts with relatively uniform fiber length would be more difficult to detect. Determining whether these regions demonstrating even declines regardless of fiber size are the result of sex differences in fiber composition or an early stage of decline shared across tracts will require further histological examination.

A driving source of this sex discrepancy may be the hormonal effects of menopause in female subjects, as the impact of menopause on the brain have been demonstrated to include structural, connectivity, and metabolic effects. While cognitive effects appear to stabilize post-menopause, this is likely due to compensatory adaptive processes rather than structural restoration (Mosconi et al., 2021). Our results likely capture structural effects of peri-menopause and post-menopause on the aging WM. A more thorough understanding of the underlying variables driving tract differences in the interaction between microstructural and morphometric declines may benefit both our understanding of aging

trajectories in general, and potentially aid in the development of interventions for specific influences on neurological health such as menopause.

Age-lagged morphometry-microstructure relationships

Results from the CCF analysis demonstrated that declines in morphometry and microstructure were largely contemporaneous, with the only notable exception to this pattern being the CCG, in which tract $length_{perc}$ changes appear to lead changes in FA_{perc}. The general commonality of declines between morphometric and microstructural declines can be taken as a representation of the shared mechanisms of decline between the two sets of measures, as declines in both are theoretically based on the deterioration and culling of axon fibers. While it seems intuitive that this degeneration would results in microstructural changes prior to morphometric declines, the measurement sensitivity necessarily to identify significant microstructural changes likely results in a non-negligible delay in our ability to detect these declines.

Conclusions

Both morphometry and microstructure analyzed in this study depict WM age-related differences as highly tract-specific, sex specific, and varied across the aging brain. Broad whole-WM effects supported our expectations for normalized volume and length decreases with age, along with anticipated microstructural declines. Examining VLR revealed additional patterns in age-related WM change consistent with our predictions. To our knowledge, this is the first study to incorporate in-vivo WM tract length differences in healthy aging.

Additionally, these findings demonstrate the predominance of crossing WM fibers in the measurement of WM integrity using dMRI. TRACULA provides a valuable tool to map the morphometric changes in our tracts of interest, but the microstructural values measured within those regions are nonetheless influenced by the fibers of other tracts and radiations not included in this model. These contributions must be taken into account when examining tract-based microstructural changes. Our findings suggest that predominantly prefrontal and inferior-frontal regions demonstrate a greater degree of degeneration in crossing WM fibers, notable in our findings in the Fminor, ILF, and UNC, suggesting these regions are broadly more susceptible to decline.

Complicating the task of modeling age-related WM changes is the apparent presence of additional factors in determining which tracts exhibit specific patterns of decline both across and between sexes. These trends cannot be fully accounted for by observed micro-/macrostructural interactions. Additional microstructural and histological variables will need to be incorporated into future models. An area of considerable interest to this study is the exploration of WM perfusion. Imaging of regional perfusion in the WM is a relatively novel capability with observed relationships to WM integrity (Chen et al., 2013;

Kim et al., 2020). Regional differences in WM perfusion may represent a missing piece in our understanding of age-related WM declines as a whole.

REFERENCES

Armstrong, C. L., Traipe, E., Hunter, J. V., Haselgrove, J. C., Ledakis, G. E., Tallent, E. M., Shera, D., & van Buchem, M. A. (2004). Age-related, regional, hemispheric, and medial-lateral differences in myelin integrity in vivo in the normal adult brain. *AJNR. American Journal of Neuroradiology*, *25*(6), 977–984.

Armstrong, N. M., An, Y., Shin, J. J., Williams, O. A., Doshi, J., Erus, G., Davatzikos, C., Ferrucci, L., Beason-Held, L. L., & Resnick, S. M. (2020). Associations between cognitive and brain volume changes in cognitively normal older adults. *NeuroImage*, *223*, 117289.

Avellino, A. M., Hart, D., Dailey, A. T., MacKinnon, M., Ellegala, D., & Kliot, M. (1995). Differential macrophage responses in the peripheral and central nervous system during wallerian degeneration of axons. *Experimental Neurology*, *136*(2), 183–198.

Azevedo, C. J., Cen, S. Y., Jaberzadeh, A., Zheng, L., Hauser, S. L., & Pelletier, D. (2019). Contribution of normal aging to brain atrophy in MS. *Neurology(R) Neuroimmunology & Neuroinflammation*, *6*(6). https://doi.org/10.1212/NXI.0000000000000616

Bajada, C. J., Schreiber, J., & Caspers, S. (2019). Fiber length profiling: A novel approach to structural brain organization. *NeuroImage*, *186*, 164–173.

Baker, L. M., Laidlaw, D. H., Cabeen, R., Akbudak, E., Conturo, T. E., Correia, S., Tate, D. F., Heaps-Woodruff, J. M., Brier, M. R., Bolzenius, J., Salminen, L. E., Lane, E. M., McMichael, A. R., & Paul, R. H. (2017). Cognitive reserve moderates the relationship between neuropsychological performance and white matter fiber bundle length in healthy older adults. *Brain Imaging and Behavior*, *11*(3), 632–639.

Baker, L. M., Laidlaw, D. H., Conturo, T. E., Hogan, J., Zhao, Y., Luo, X., Correia, S., Cabeen, R., Lane, E. M., Heaps, J. M., Bolzenius, J., Salminen, L. E., Akbudak, E., McMichael, A. R., Usher, C., Behrman, A., & Paul, R. H. (2014). White matter changes with age utilizing quantitative diffusion MRI. *Neurology*, *83*(3), 247–252.

Bartzokis, G. (2004). Age-related myelin breakdown: a developmental model of cognitive decline and Alzheimer's disease. *Neurobiology of Aging*, *25*(1), 5–18; author reply 49–62.

Bastin, M. E., Muñoz Maniega, S., Ferguson, K. J., Brown, L. J., Wardlaw, J. M., MacLullich, A. M. J., & Clayden, J. D. (2010). Quantifying the effects of normal ageing on white matter structure using unsupervised tract shape modelling. *NeuroImage*, *51*(1), 1–10.

Benitez, A., Jensen, J. H., Falangola, M. F., Nietert, P. J., & Helpern, J. A. (2018). Modeling white matter tract integrity in aging with diffusional kurtosis imaging. *Neurobiology of Aging*, *70*, 265–275.

Bookheimer, S. Y., Salat, D. H., Terpstra, M., Ances, B. M., Barch, D. M., Buckner, R. L., Burgess, G. C., Curtiss, S. W., Diaz-Santos, M., Elam, J. S., Fischl, B., Greve, D. N., Hagy, H. A., Harms, M. P., Hatch, O. M., Hedden, T., Hodge, C., Japardi, K. C., Kuhn, T. P., … Yacoub, E. (2019). The Lifespan Human Connectome Project in Aging: An overview. *NeuroImage*, *185*, 335–348.

Brickman, A. M., Meier, I. B., Korgaonkar, M. S., Provenzano, F. A., Grieve, S. M., Siedlecki, K. L., Wasserman, B. T., Williams, L. M., & Zimmerman, M. E. (2012). Testing the white matter retrogenesis hypothesis of cognitive aging. *Neurobiology of Aging*, *33*(8), 1699–1715.

Chen, J. J., Rosas, H. D., & Salat, D. H. (2013). The relationship between cortical blood flow and sub-cortical white-matter health across the adult age span. *PloS One*, *8*(2), e56733.

Choy, S. W., Bagarinao, E., Watanabe, H., Ho, E. T. W., Maesawa, S., Mori, D., Hara, K., Kawabata, K., Yoneyama, N., Ohdake, R., Imai, K., Masuda, M., Yokoi, T., Ogura, A., Taoka, T., Koyama, S., Tanabe, H. C., Katsuno, M., Wakabayashi, T., … Sobue, G. (2020). Changes in white matter fiber density and morphology across the adult lifespan: A cross-sectional fixel-based analysis. *Human Brain Mapping*, *41*(12), 3198–3211.

Debette, S., & Markus, H. S. (2010). The clinical importance of white matter hyperintensities on brain magnetic resonance imaging: systematic review and meta-analysis. *BMJ* , *341*, c3666.

de Groot, M., Cremers, L. G. M., Ikram, M. A., Hofman, A., Krestin, G. P., van der Lugt, A., Niessen, W. J., & Vernooij, M. W. (2016). White Matter Degeneration with Aging: Longitudinal Diffusion MR Imaging Analysis. *Radiology*, *279*(2), 532–541.

de Groot, M., Ikram, M. A., Akoudad, S., Krestin, G. P., Hofman, A., van der Lugt, A., Niessen, W. J., & Vernooij, M. W. (2015). Tract-specific white matter degeneration in aging: the Rotterdam Study. *Alzheimer's & Dementia: The Journal of the Alzheimer's Association*, *11*(3), 321–330.

Fan, Q., Nummenmaa, A., Witzel, T., Ohringer, N., Tian, Q., Setsompop, K., Klawiter, E. C., Rosen, B. R., Wald, L. L., & Huang, S. Y. (2020). Axon diameter index estimation independent of fiber orientation distribution using high-gradient diffusion MRI. *NeuroImage*, *222*, 117197.

Fan, Q., Tian, Q., Ohringer, N. A., Nummenmaa, A., Witzel, T., Tobyne, S. M., Klawiter, E. C., Mekkaoui, C., Rosen, B. R., Wald, L. L., Salat, D. H., & Huang, S. Y. (2019). Age-related alterations in axonal microstructure in the corpus callosum measured by high-gradient diffusion MRI. *NeuroImage*, *191*, 325–336.

Fjell, A. M., McEvoy, L., Holland, D., Dale, A. M., Walhovd, K. B., & Alzheimer's Disease Neuroimaging Initiative. (2014). What is normal in normal aging? Effects of aging, amyloid and Alzheimer's disease on the cerebral cortex and the hippocampus. *Progress in Neurobiology*, *117*, 20–40.

Fjell, A. M., Walhovd, K. B., Fennema-Notestine, C., McEvoy, L. K., Hagler, D. J., Holland, D., Brewer, J. B., & Dale, A. M. (2009). One-year brain atrophy evident in healthy aging. *The Journal of Neuroscience: The Official Journal of the Society for Neuroscience*, *29*(48), 15223–15231.

Grotheer, M., Rosenke, M., Wu, H., Kular, H., Querdasi, F. R., Natu, V. S., Yeatman, J. D., & Grill-Spector, K. (2022). White matter myelination during early infancy is linked to spatial gradients and myelin content at birth. *Nature Communications*, *13*(1), 997.

Harms, M. P., Somerville, L. H., Ances, B. M., Andersson, J., Barch, D. M., Bastiani, M., Bookheimer, S. Y., Brown, T. B., Buckner, R. L., Burgess, G. C., Coalson, T. S., Chappell, M. A., Dapretto, M., Douaud, G., Fischl, B., Glasser, M. F., Greve, D. N., Hodge, C., Jamison, K. W., … Yacoub, E. (2018). Extending the Human Connectome Project across ages: Imaging protocols for the Lifespan Development and Aging projects. *NeuroImage*, *183*, 972–984.

Hoagey, D. A., Rieck, J. R., Rodrigue, K. M., & Kennedy, K. M. (2019). Joint contributions of cortical

morphometry and white matter microstructure in healthy brain aging: A partial least squares correlation analysis. *Human Brain Mapping*, *40*(18), 5315–5329.

Huang, H., Xue, R., Zhang, J., Ren, T., Richards, L. J., Yarowsky, P., Miller, M. I., & Mori, S. (2009). Anatomical characterization of human fetal brain development with diffusion tensor magnetic resonance imaging. *The Journal of Neuroscience: The Official Journal of the Society for Neuroscience*, *29*(13), 4263–4273.

Huang, S. Y., Tian, Q., Fan, Q., Witzel, T., Wichtmann, B., McNab, J. A., Daniel Bireley, J., Machado, N., Klawiter, E. C., Mekkaoui, C., Wald, L. L., & Nummenmaa, A. (2020). High-gradient diffusion MRI reveals distinct estimates of axon diameter index within different white matter tracts in the in vivo human brain. *Brain Structure & Function*, *225*(4), 1277–1291.

Hu, H.-Y., Ou, Y.-N., Shen, X.-N., Qu, Y., Ma, Y.-H., Wang, Z.-T., Dong, Q., Tan, L., & Yu, J.-T. (2021). White matter hyperintensities and risks of cognitive impairment and dementia: A systematic review and meta-analysis of 36 prospective studies. *Neuroscience and Biobehavioral Reviews*, *120*, 16–27.

Kezele, I. B., Arnold, D. L., & Collins, D. L. (2008). Atrophy in white matter fiber tracts in multiple sclerosis is not dependent on tract length or local white matter lesions. *Multiple Sclerosis* , *14*(6), 779–785.

Kiely, M., Triebswetter, C., Cortina, L. E., Gong, Z., Alsameen, M. H., Spencer, R. G., & Bouhrara, M. (2022). Insights into human cerebral white matter maturation and degeneration across the adult lifespan. *NeuroImage*, *247*, 118727.

Kim, C.-M., Alvarado, R. L., Stephens, K., Wey, H.-Y., Wang, D. J. J., Leritz, E. C., & Salat, D. H. (2020). Associations between cerebral blood flow and structural and functional brain imaging measures in individuals with neuropsychologically defined mild cognitive impairment. *Neurobiology of Aging*, *86*, 64–74.

Kodiweera, C., Alexander, A. L., Harezlak, J., McAllister, T. W., & Wu, Y.-C. (2016). Age effects and sex differences in human brain white matter of young to middle-aged adults: A DTI, NODDI, and q-space study. *NeuroImage*, *128*, 180–192.

Liewald, D., Miller, R., Logothetis, N., Wagner, H.-J., & Schüz, A. (2014). Distribution of axon diameters in cortical white matter: an electron-microscopic study on three human brains and a macaque. *Biological Cybernetics*, *108*(5), 541–557.

Madden, D. J., Bennett, I. J., Burzynska, A., Potter, G. G., Chen, N.-K., & Song, A. W. (2012). Diffusion tensor imaging of cerebral white matter integrity in cognitive aging. *Biochimica et Biophysica Acta*, *1822*(3), 386–400.

Maffei, C., Lee, C., Planich, M., Ramprasad, M., Ravi, N., Trainor, D., Urban, Z., Kim, M., Jones, R. J., Henin, A., Hofmann, S. G., Pizzagalli, D. A., Auerbach, R. P., Gabrieli, J. D. E., Whitfield-Gabrieli, S., Greve, D. N., Haber, S. N., & Yendiki, A. (2021). Using diffusion MRI data acquired with ultra-high gradients to improve tractography in routine-quality data. In *bioRxiv* (p. 2021.06.28.450265). https://doi.org/10.1101/2021.06.28.450265

Marner, L., Nyengaard, J. R., Tang, Y., & Pakkenberg, B. (2003). Marked loss of myelinated nerve fibers in the human brain with age. *The Journal of Comparative Neurology*, *462*(2), 144–152.

Mosconi, L., Berti, V., Dyke, J., Schelbaum, E., Jett, S., Loughlin, L., Jang, G., Rahman, A., Hristov, H., Pahlajani, S., Andrews, R., Matthews, D., Etingin, O., Ganzer, C., de Leon, M., Isaacson, R., & Brinton, R. D. (2021). Menopause impacts human brain structure, connectivity, energy metabolism, and amyloid-beta deposition. *Scientific Reports*, *11*(1), 10867.

Ouyang, Y., Cui, D., Yuan, Z., Liu, Z., Jiao, Q., Yin, T., & Qiu, J. (2021). Analysis of Age-Related White Matter Microstructures Based on Diffusion Tensor Imaging. *Frontiers in Aging Neuroscience*, *13*, 664911.

Pakkenberg, B., & Gundersen, H. J. (1997). Neocortical neuron number in humans: effect of sex and age. *The Journal of Comparative Neurology*, *384*(2), 312–320.

Piguet, O., Double, K. L., Kril, J. J., Harasty, J., Macdonald, V., McRitchie, D. A., & Halliday, G. M. (2009). White matter loss in healthy ageing: a postmortem analysis. *Neurobiology of Aging*, *30*(8), 1288–1295.

Sala, S., Agosta, F., Pagani, E., Copetti, M., Comi, G., & Filippi, M. (2012). Microstructural changes and

atrophy in brain white matter tracts with aging. *Neurobiology of Aging*, *33*(3), 488–498.e2.

Seiler, S., Fletcher, E., Hassan-Ali, K., Weinstein, M., Beiser, A., Himali, J. J., Satizabal, C. L., Seshadri, S., DeCarli, C., & Maillard, P. (2018). Cerebral tract integrity relates to white matter hyperintensities, cortex volume, and cognition. *Neurobiology of Aging*, *72*, 14–22.

Stadlbauer, A., Salomonowitz, E., Strunk, G., Hammen, T., & Ganslandt, O. (2008). Age-related degradation in the central nervous system: assessment with diffusion-tensor imaging and quantitative fiber tracking. *Radiology*, *247*(1), 179–188.

Taha, H. T., Chad, J. A., & Chen, J. J. (2022). DKI enhances the sensitivity and interpretability of age-related DTI patterns in the white matter of UK biobank participants. *Neurobiology of Aging*, *115*, 39–49.

Taki, Y., Kinomura, S., Sato, K., Goto, R., Wu, K., Kawashima, R., & Fukuda, H. (2011). Correlation between gray/white matter volume and cognition in healthy elderly people. *Brain and Cognition*, *75*(2), 170–176.

Tang, Y., Nyengaard, J. R., Pakkenberg, B., & Gundersen, H. J. (1997). Age-induced white matter changes in the human brain: a stereological investigation. *Neurobiology of Aging*, *18*(6), 609–615.

Uddin, M. N., Figley, T. D., Solar, K. G., Shatil, A. S., & Figley, C. R. (2019). Comparisons between multi-component myelin water fraction, T1w/T2w ratio, and diffusion tensor imaging measures in healthy human brain structures. *Scientific Reports*, *9*(1), 2500.

Wu, H., Sun, C., Huang, X., Wei, R., Li, Z., Ke, D., Bai, R., & Liang, H. (2022). Short-Range Structural Connections Are More Severely Damaged in Early-Stage MS. *AJNR. American Journal of Neuroradiology*, *43*(3), 361–367.

Yeatman, J. D., Wandell, B. A., & Mezer, A. A. (2014). Lifespan maturation and degeneration of human brain white matter. *Nature Communications*, *5*, 4932.

Yendiki, A., Panneck, P., Srinivasan, P., Stevens, A., Zöllei, L., Augustinack, J., Wang, R., Salat, D., Ehrlich, S., Behrens, T., Jbabdi, S., Gollub, R., & Fischl, B. (2011). Automated probabilistic reconstruction of white-matter pathways in health and disease using an atlas of the underlying

anatomy. *Frontiers in Neuroinformatics*, *5*, 23.